**Manuscript full title**:

The distinct problems of physical inconsistency and of multivariate bias potentially involved in the statistical adjustment of climate simulations

**Running head (short title)**:

Physical inconsistency versus multivariate bias

**Name and affiliation of each author**:

Mégane Alavoine[1], and Patrick Grenier[1,2]

[1]*Centre pour l'Étude et la Simulation du Climat à l'Échelle Régionale* (ESCER), *Université du Québec à Montréal*, Montréal, Québec, Canada

[2]Ouranos, Montréal, Québec, Canada

**Corresponding author address and e-mail**:

Patrick Grenier
Université du Québec à Montréal – Centre ESCER
Pavillon Président-Kennedy – local PK-6151
201, avenue du Président-Kennedy
Montréal (QC)
H2X 3Y7, Canada
grenier.patrick.2@courrier.uqam.ca

**Keywords**: climate simulations; physical relationships; statistical biases; multivariate adjustment techniques; air humidity.

**Abstract**

Bias adjustment of numerical climate model simulations involves several technical and epistemological arguments wherein the notion of physical inconsistency is often referred to, either for rejecting the legitimacy of bias adjustment in general or for justifying the necessity of sophisticated multivariate techniques. However, this notion is often mishandled, in part because the literature generally proceeds without defining it. In this context, the central objective of this study is to clarify and illustrate the distinction between physical inconsistency and multivariate bias, by investigating the effect of bias adjustment on two different kinds of inter-variable relationships, namely a physical constraint expected to hold at every step of a time series and statistical properties that emerge with potential bias over a climatic time scale. The study involves the application of 18 alternative bias adjustment techniques on 10 climate simulations and over 12 sites across North America. Adjusted variables are temperature, pressure, relative humidity and specific humidity, linked by a thermodynamic constraint. The analysis suggests on the one hand that a clear instance of potential physical inconsistency can be avoided with either a univariate or a multivariate technique, if and only if the bias adjustment strategy explicitly considers the physical constraint to be preserved. On the other hand, it also suggests that sophisticated multivariate techniques alone aren't complete adjustment strategies in presence of a physical constraint, as they cannot replace its explicit consideration. As a supplementary objective, this study relates common optional adjustment procedures with likely effects on diverse basic statistical properties, as an effort to guide climate information users in the determination of adequate bias adjustment strategies for their research purposes.

## 1. Introduction

Supply and demand for climate information have been continuous and arguably growing for decades (Hecht 1984; Lourenço et al., 2016; Lugen 2020; Findlater et al., 2021). In this sector of activity, simulations from physics-based global and regional climate models (GCMs and RCMs) play an important role, models being generally viewed as the best source for plausible values of future change in key climate variables (Flato et al., 2013). Yet, simulated statistical properties such as averages, extreme values and inter-variable correlations often show differences relative to observation-based reference products over the recent past. Therefore, it is often necessary to adjust simulations before using them, for example in impact models or for estimating plausible evolutions in threshold-dependent climate indices (Maraun et al., 2017; Lanzante et al. 2018; Zscheischler et al., 2019; Martins et al., 2021).

There exist at least four potential sources for reference-simulation statistical differences, which are not easy to disentangle and whose relative roles are context-dependent: 1) mismatch in spatial representativeness (scale, grid location and/or altitude); 2) imperfections in climate models' physics formulation; 3) imperfections in reference products; and 4) non-synchronicity between real and simulated natural fluctuations over long time scales (e.g., Addor and Fischer, 2015; Chen et al., 2016; Diaconescu et al., 2017; Kotlarski et al., 2019). In operational climate services, the third and fourth sources are often found or assumed to play lesser roles, and differences are often managed by means of a single joint statistical technique addressing simultaneously scale mismatch as well as biases stemming from GCMs' and RCMs' imperfect physics (e.g., Wilcke et al., 2013; Gennaretti et al., 2015; Lehtonen et al., 2016). In such cases (and in this study), expressions like 'bias adjustment' and 'bias correction' are thus convenient misnomers, as the involved technique is in fact dealing with more than the sole bias problem. It must also be emphasized that the bias problem is *a priori* potential, as there exist contexts (i.e., specific simulation, location, variable and statistical property) where reference and raw simulated time series match relatively well (for a mixture of right and wrong reasons). In such contexts, a suitable adjustment technique is expected to leave raw data essentially untouched (adding ~ 0 or multiplying by ~ 1).

A distinct problem involved in the use of climate simulations is the risk of generating physical inconsistency (PI) through the adjustment technique. Here the concept is used in the sense of internal or external inconsistency, occurring when a theory, a model or a description is self-contradictory or contradicts theories in neighbor fields, in line with how it is used in traditional philosophy of science (e.g., Kuhn 1977; Laudan, 1984; Steel 2010). In the context of climate simulation bias adjustment, one illustrative example would be the breaking of the thermodynamic relationship between temperature ($T$), pressure ($P$), specific humidity ($q$) and relative humidity (RH). This specific relationship has already been used to illustrate how PI may be generated by a typical univariate bias adjustment algorithm (Grenier, 2018), and the present study extends the methodology notably to multivariate algorithms. The nomenclature of Grenier (2018) refers to PI of type 1 when an out-of-range value is attributed to an individual variable (hence contradicting the very meaning of the variable), and to PI of type 2 when several variables have values collectively contradicting their meanings or contradicting a well-credentialed element of physics (while each individual value may respect its range).

Normally, raw simulations are devoid of many potential instances of such inconsistencies, as relevant physics elements are precisely targeted as building blocks for climate models (Jacobson, 2005; Laprise, 2008; Winsberg 2018; Hewitt et al., 2021), but exceptions linked with numerical artefacts may occur (Laprise, 2008; Ruosteenoja et al., 2017). Investigating the potential PI problem having in mind the model-as-a-whole (rather than specific constitutive elements) would be a dead-end, as there would be no other science to be consistent or inconsistent with. Indeed, physics does not generate numerical climate models, but rather fundamental principles and relationships that climate modelers select and combine, along with less principled considerations (discretization schemes, parameterizations, domain management). Moreover, in the context of bias adjustment it is worth recalling that climate models are known *a priori* not to be in isomorphism with the real world (see: Petersen 2000; Parker, 2009; Giere, 2010; Lehnard and Winsberg, 2010), which rules out the argument that so-called model internal consistency does confer full physical consistency to simulated long-term statistics (this argument is often used against bias adjustment legitimacy). Current models and simulations are *based on* physics, but not *holistically consistent with* physics.

Framed this way, the physical inconsistency (PI) problem is distinguished from the bias problem in at least two important ways. First, PI is identified from individual time steps and grid tiles. For example, PI instantiated by daily minimal temperature exceeding the maximal daily temperature ($T_{\mathrm{min}} > T_{\mathrm{max}}$) would be diagnosed for each day separately (Thrasher et al., 2012; Agbazo and Grenier, 2019). In contrast, a bias concerns statistics (either univariate or multivariate) computed from a large number of time steps.

Secondly, PI is tied to a particular definition or to a specific element of physics. For example, occurrences of adjusted RH (with respect to liquid water) substantially exceeding 100 % could be viewed as physically inconsistent for Earth's atmosphere, because the aerosol load is known as sufficient to host condensation whenever supersaturation occurs (Pruppacher and Klett, 1997). Current models generally do not resolve detailed aerosol-water processes, but typical parameterizations of cloud properties attribute meaningful roles to the 100 % threshold (e.g., Del Genio et al., 1996). In contrast, a 30-year bias in a RH time series could hardly be linked to any well-identified physics element, as it emerges from the model-as-a-whole. These distinctions are excluded from several concurrent (and generally implicit) definitions of the expression 'physical inconsistency' in the context of bias adjustment. For example, some authors implicitly tag this expression (or synonyms) onto any alteration of simulated multivariate statistical dependencies (e.g., Chen et al., 2016; Sippel et al., 2016; Gómez-Navarro et al., 2018), whereas, in a rather contrary perspective, others implicitly tag this expression onto simulated gaps relative to reference multivariate properties (e.g., Vrac and Friederichs, 2015).

There exists a quasi-continuum of bias adjustment techniques, including complex ones that combine several more basic mathematical-numerical procedures. Techniques differ notably by the statistical properties they adjust, by options like attempting (or not) to preserve the simulated long-term trend, and by how days (or other temporal units) are grouped within the adjustment technique. One popular procedure is quantile mapping (QM), which adjusts the shape of simulated distributions in a univariate way (e.g., Lehtonen et al., 2016; Martins et al., 2021). The central idea of this procedure is to build a transfer function mapping the simulated onto the reference distribution over a calibration period, and then to apply it on any wanted simulation segment. Many multivariate extensions have been developed during the last decade, for purposes that also require inter-variable and/or inter-site correlations to be adjusted (e.g., Su et al., 2020). These can consist of strategic successive conditional applications of univariate QM (e.g., Piani and Haerter, 2012), or in complementing univariate QM with another procedure to adjust inter-variable dependences as well, resorting for example to shuffling (e.g., Vrac, 2018), to eigenvector-based geometric transformations (e.g., Hnilica et al., 2017), or to a complex mix of akin procedures (e.g., Cannon, 2018). Each technique is adequate when the final purpose requires its specific constitutive procedures to be activated.

In this context, the central objective of this study is to clarify and illustrate the distinction between the bias problem and the physical inconsistency problem, notably by showing that multivariate bias adjustment procedures do have the potential to break a fixed thermodynamic relationship while adjusting inter-variable correlations fairly well. To this end, 18 alternative bias adjustment techniques are applied on 10 daily climate simulations at 12 sites over North America. This offers a wide range of bias adjustment contexts, with adjustment alternatives obtained by crossing three univariate or multivariate options with two trend management options and with three temporal grouping options. The thermodynamic relationship used to illustrate the distinction is the same as in Grenier (2018), namely the instantaneous constraint linking temperature ($T$), pressure ($P$), specific humidity ($q$) and relative humidity (RH) for a homogeneous air parcel. Physical inconsistency is monitored following the two types (1 and 2) already mentioned, while monitoring of the statistical effects covers intra-annual cycles, inter-annual variability, inter-variable correlations, lag-1 auto-correlations and long-term climate change values. Monitoring these key statistical properties also serves a supplementary objective, namely to help bias adjustment practitioners judging whether techniques involving certain promoted procedures are adequate for specific purposes.

## 2. Data and methods

### 2.1. Data sets

Because this study essentially extends that of Grenier (2018) (from 1 to 18 bias adjustment techniques, and now including two multivariate procedures), the same data sets for near-surface temperature ($T$), pressure ($P$), relative humidity (RH) and specific humidity ($q$) have been used, namely the 1-hourly Climate Forecast System Reanalysis (CFSR; Saha et al., 2010) as the reference product, and an ensemble of ten 3-hourly simulations from phase 5 of the Coupled Model Intercomparison project (CMIP5; Taylor et al., 2012) as the time series to be adjusted. One of the simulations is dynamically downscaled with the Canadian Regional Climate Model version 5 (CRCM5; Šeparović et al, 2013). Table 1 contains identification information for all simulations as well as internal codes for convenient referencing within this study (e.g., SIM-08). Note that same-model simulations share the same data up to year 2005; therefore certain results concerning the calibration period are based on the four RCP8.5 simulations only. Time series from grid tiles including twelve different cities over North America are used, with coordinates corresponding to that of the World Meteorological Organization (WMO)'s respective stations (although station data themselves are not used; see Table 2 for more detailed site-related information). This sites selection includes tropical (Miami), arid (e.g., El Paso), temperate (e.g., Vancouver) and cold (e.g., Yellowknife) environments (Peel et al., 2007). The bias adjustment calibration period is 1981-2010, and the application period is 1981-2100. Bias adjustment temporal frequency is daily, with each day represented by its variables' values at 12 UTC. Note that all acronym expansions may be found in Appendix A.

It is worth mentioning that the selection of CFSR and of the ten simulations does not necessarily meet operational climate services concerns, such as identifying the best gridded reference product for a given purpose or adequately covering uncertainty in future climate change. This is justified by the methodological nature of this study, which focuses notably on showing how promoted multivariate bias adjustment procedures may act on simulations that are initially consistent regarding one specific thermodynamic aspect. For such a purpose, it is not necessary that the level of realism of the reference product be optimal. Moreover, the potential for generalization of the results is sufficiently addressed by covering a fair variety of climatological situations, in terms of types of climates as well as of simulated bias structures and future change values.

## 2.2. Nomenclature

For any site, reference time series are referred to as $T_{\mathrm{cfsr}}$, $P_{\mathrm{cfsr}}$, $\mathrm{RH}_{\mathrm{cfsr}}$ and $q_{\mathrm{cfsr}}$, whereas time series from any of the ten simulations are referred to as $T_{\mathrm{sim}}$, $P_{\mathrm{sim}}$, $\mathrm{RH}_{\mathrm{sim}}$ and $q_{\mathrm{sim}}$. At any time step, each of these time series respects a same thermodynamic constraint between the four variables, which can be symbolized by the pair of reverse functions $f(\cdot)$ and $g(\cdot)$ (subscript absence denotes a variable in general):

$$\mathrm{RH} = f(T, P, q) \tag{1}$$

$$q = g(T, P, \mathrm{RH}) \tag{2}$$

The function $f(\cdot)$ can be obtained through the following basic thermodynamic equations (Wallace and Hobbs, 2006):

$$\mathrm{RH} \equiv 100\, w / w_{sat} \quad (3)$$

$$w = q / (1 - q) \quad (4)$$

$$w_{sat} = 0.622\, e_{sat} / (P - e_{sat}) \quad (5)$$

where $w$ is the mixing ratio, $w_{sat}$ the saturation mixing ratio, and $e_{sat}$ the saturation partial pressure of water vapor. The empirical fit of Sonntag (1990), hereafter referred to by the subscript 'so90', has been chosen to calculate $e_{sat}$ from temperature:

$$e_{sat}(T) = 100 \exp(\mathrm{a}_1 + \mathrm{a}_2 + \mathrm{a}_3 + \mathrm{a}_4 + \mathrm{a}_5) \quad (6a)$$
$$\mathrm{a}_1 = -6096.9385\, T^{-1} \quad (6b)$$
$$\mathrm{a}_2 = 16.635794 \quad (6c)$$
$$\mathrm{a}_3 = -2.711193 \times 10^{-2}\, T \quad (6d)$$
$$\mathrm{a}_4 = 1.673952 \times 10^{-5}\, T^2 \quad (6e)$$
$$\mathrm{a}_5 = 2.433502 \ln(T) \quad (6f)$$

where $T$ is in kelvins and $e_{sat}$ in pascals. The constraint $g(\cdot)$ is straightforwardly obtained by isolating $q$ in the system of equations (3) to (5) and using the same empirical fit for $e_{sat}(T)$. Because reanalysis or model outputs (for $T$, $P$, RH and $q$) may possibly not respect this $f(\cdot)$ relationship, due either to the use of another empirical fit or to a univariate extrapolation to approximate the near-surface variables from the lowest model level (Ruosteenoja et al., 2017; Grenier, 2018), RH has been recalculated with $f(\cdot)$ for all situations, and new values exceeding 100% have been capped at this threshold, with corresponding $q$ values recalculated with $g(\cdot)$. Hence, time series that serve as input to the adjustment techniques are consistent regarding $f(\cdot)$ or $g(\cdot)$ at each time step, assuming that the involved variables represent instantaneous and spatially homogeneous quantities. Also, the study assumes RH with respect to liquid water, even for temperatures below the freezing point.

Time series directly obtained from the application of any of the 18 bias adjustment techniques (described in Section 2.3) are referred to as $T_{ba}$, $P_{ba}$, $\mathrm{RH}_{ba}$ and $q_{ba}$. Connections between simulated and adjusted quantities are schematized in Figure 1. Among the tested techniques, 6 are univariate and 12 are multivariate, and the diagram distinguishes these two classes of alternatives by subdividing the 'ba' subscript into 'uni' (univariate procedure) and 'multi' (joint procedure); the latter subscripts are only used in Figure 1. After direct bias adjustment, the quantities $q_{\mathrm{so90}}$ and $\mathrm{RH}_{\mathrm{so90}}$ are calculated through the relations

$$\mathrm{RH}_{so90} \equiv f(T_{ba}, P_{ba}, q_{ba}) \tag{7}$$

$$q_{\mathrm{so90}} \equiv g(T_{ba}, P_{ba}, \mathrm{RH}_{ba}) \tag{8}$$

to meet the methodological objectives presented in Section 2.4.

## 2.3. Bias adjustment

The 18 alternative adjustment techniques are obtained by crossing three options related to dimensionality (either univariate, shuffling-based bivariate or eigenvector-based quadrivariate) with two options related to long-term trend management (either free to evolve or tentatively preserved through the isolation of a regression) and with three options related to temporal grouping of the daily values (either annual, monthly or resorting to a moving window). Quantile mapping (QM) is a procedure common to all alternatives, as this corresponds to a univariate step also embedded into the multivariate techniques. The QM step is performed with additive (by contrast with multiplicative) transfer functions in all cases, as variables RH and $q$ (bounded by 0 and 1) are transformed into their logit function [of general form: $y = \ln(x / (1-x))$] prior to bias adjustment, and inversely transformed through the sigmoid function [of general form: $x = 1/(1+\exp(-y))$] at the end.

The bias adjustment algorithm is schematized in Figure 2. The first computing step is variable categorization, whereby a variable is either kept as is if its typical distribution is disconnected from any physical bounds (like $T$ and $P$), transformed into its logarithm if lower-bounded at zero while there is no upper bound (this would be the case for precipitation), transformed into its logit function if it is bounded within 0 and 1 (like RH and $q$), or normalized prior to logit transformation if the upper bound is not fixed (this would be the case for incoming solar radiation). This pragmatic categorization, schematized in

Figure 3, expands upon an already proposed recourse to the logit transformation (Cannon, 2018), and its rationale is to prevent occurrence of type 1 (out-of-bound) physical inconsistency for directly adjusted variables. Next comes the decision for temporal grouping of the days. The 'annual' option uses a single transfer function ($F_{\mathrm{QM}}$) for all days of the time series, the 'monthly' option uses for example an $F_{\mathrm{QM}}$ based on 900 days for April (30 days in this month, times 30 calibration years over 1981-2010), and the '(moving) window' option starts for example with a first $F_{\mathrm{QM}}$ based on 930 days for January 1$^{st}$ (31 days from December 17$^{th}$ to January 16$^{th}$, times 30 calibration years). The next decision in the algorithm is whether $F_{\mathrm{QM}}$ is applied on complete values, hence letting the simulated long-term trend free to evolve as a consequence of the quantile-dependent character of the bias to adjust (Gobiet et al., 2015), or if there is rather a trend preservation (TP) attempt, by which a regression is isolated for letting the core of the algorithm (QM plus optional multivariate procedure) operate on the residuals (Hempel et al., 2013; Agbazo and Grenier, 2019). The TP procedure resorts to a local regression (Cleveland, 1979). Finally comes the core of the algorithm, followed by reverse steps such as adding back the regression (if the trend preservation option was activated) and transforming back the logit function (for RH and $q$).

The core of the algorithm corresponds to the dimensionality option, namely to a choice between the univariate and one of the two multivariate possibilities. The univariate option simply consists of applying QM on the values selected by prior options (temporal grouping, and either the complete values or the residuals around the isolated regression). The $F_{\mathrm{QM}}$ is defined at 52 nodes (percentiles 0, 1, 3, …, 97, 99 and 100). QM is widely applied in climate studies, under different variants and names, and further details as well as implications have been described notably by Themeβl et al. (2012), Wilcke et al. (2013) and Gennaretti et al. (2015).

The first multivariate option resorts to the shuffling procedure, used and explained notably by Vrac (2018). Here univariate QM is first applied on each variable separately, and $T$ is chosen as the master (unshuffled) variable on which to align each of the other variables (separately, in a bivariate fashion) in order to obtain the reference inter-variable Spearman correlation coefficients. Shuffling is a time-exchange of individual values within the time series, thus durations of the application and the calibration periods must be the same. Shuffling-based techniques hence require the application period to be covered through four successive and subsequently concatenated blocks (1981-2010, 2011-2040, 2041-2070 and 2071-2100). For the window option, implementing the shuffling is conceptually more challenging than what was done by Vrac (2018), because a choice has to be made between shuffling all values involved in the construction of the current $F_{QM}$ (the width of the window is 31 days), or shuffling only the currently processed day-of-the-year; the latter option was retained, to ensure each simulated day is "reflected" somewhere in the final adjusted time series.

The second multivariate option resorts to eigenvectors for geometrically translating, rotating and resizing altogether the simulated distributions to match the reference ones (in a quadrivariate fashion). This procedure is described by Hnilica et al. (2017) in the context of a precipitation multi-site application (here each study site is processed separately). The Matlab® *eig*(·) function is used, and the problem of arbitrariness in the eigenvector orientations described by Hnilica et al. (2017) is addressed by computing all sixteen ($2^4$) orientation possibilities and retaining the one for which the sum of the four (univariate) correlation coefficients between the simulated and the adjusted series was larger. In rare cases, the retained solution incorporated negative coefficients, which prompted systematic visual inspection of the results. The procedure is followed by a QM procedure, as visual inspection showed that such guardrail can rectify univariate results that are otherwise unstable, again in rare cases.

Hereinafter, the labels 'QM-only', 'QM-shuf' and 'eig-QM' will refer respectively to the six univariate, the six shuffling-based and the six eigenvector-based techniques, either in general or for a specific alternative if the auxiliary options are also specified. Each technique corresponds to a row in Table 3, which is discussed in Section 4 as a synthesis of the results.

## 2.4. Overarching methodology

### *a. Physical inconsistency*

To investigate whether a bias adjustment technique does cause inter-variable physical inconsistency (PI), $q_{so90}$ is compared with $q_{ba}$ (see Figure 1). Because $q_{so90}$ is a quantity defined to be consistent with $T_{ba}$, $P_{ba}$ and $RH_{ba}$, any discrepancy between $q_{so90}$ and $q_{ba}$ would indicate a breaking of the clear instance of inter-variable thermodynamic consistency expressed by $f(\cdot)$ or $g(\cdot)$. As PI is assessed at individual time steps, there is, for each adjustment alternative, each simulation and each study site, a total of 43,800 test occasions (120 years for the application period x 365 days per year). Related results will tell whether this specific instance of thermodynamic consistency survives bias adjustment, when the adjustment strategy does not explicitly prescribe it.

It will also be investigated whether $RH_{so90}$ can exceed 100 %. The directly adjusted quantity $RH_{ba}$ cannot exceed this threshold because of the logit transformation, but there is no such guarantee for $RH_{so90}$. Related results could give insight, in case bias adjustment is shown not to preserve thermodynamic consistency, about whether it is RH or $q$ that should be explicitly calculated from the three other directly adjusted variables, in order to respect $f(\cdot)$ and $g(\cdot)$.

*b. Statistical properties*

The bias problem relates to long-term statistics, either univariate or multivariate, and the point of rendering an algorithm multivariate is to adjust inter-variable statistical dependencies. When the various mathematical-numerical procedures promoted in the scientific literature to achieve this specific objective (e.g., Piani and Haerter, 2012; Hnilica et al., 2017; Vrac, 2018, Cannon, 2018) are used in conjunction with auxiliary procedures (e.g., trend preservation, moving window, logit transformation, multiscale adjustment), a slight undoing of the work of first-acting procedures can occur, hence rendering the final effect on several relevant statistical properties not always obvious *a priori*. Therefore, the following properties (with related test metrics) are systematically monitored: annual cycle (through visual inspection); inter-annual variability (with 30-yr standard deviations of intra-month averages); inter-variable correlation (with 30-yr averages of intra-month Spearman rank coefficients); lag-1 auto-correlation (with 30-yr averages of intra-month Spearman rank coefficients); and climate change values (with so-called Δ, from 1981-2010 to 2071-2100).

## 3. Results and analysis

### 3.1. Physical inconsistency

The effect of bias adjustment on inter-variable physical consistency is investigated by comparing $q_{ba}$ (the $q$ value directly obtained with adjustment) and $q_{so90}$ (the $q$ value it takes to be consistent with $T_{ba}$, $P_{ba}$ and $RH_{ba}$). Results for one study site (Montreal) are presented in Figure 4, for all dimensionality options

(‘QM-only’, ‘QM-shuf’ or ‘eig-QM’) crossed with all grouping options (‘annual’, ’monthly’ or ‘window’); trend preservation (TP) is activated for all panels (deactivating it led to similar results). Each individual time step from each simulation provides a count, for a sum of 438,000 counts per panel. Results show noticeable discrepancies from the 1:1 ratio line for all techniques, hence indicating a breaking of the inter-variable thermodynamic consistency expressed by $f(\cdot)$ or $g(\cdot)$. Some techniques show lower RMSE (between $q_{ba}$ and $q_{so90}$) than the others, but it is clear that procedures developed for adjusting 30-year inter-variable dependencies are not made to preserve thermodynamic consistency at specific time steps. The relationship $f(\cdot)$ or $g(\cdot)$ must hence be instructed explicitly within the adjustment strategy. Selecting $q_{so90}$ instead of $q_{ba}$ could however lead to increased residual biases for the $q$ variable. Among 10,368 cases (18 alternatives x 12 sites x 12 months x 4 RCP8.5 simulations), $q_{so90}$ distributions are more biased (with respect to $q_{cfsr}$) than their corresponding $q_{ba}$ distribution with a frequency of 69.3 %, and less biased than their corresponding initial $q_{sim}$ distribution with a frequency of 89.5 % (using the Kolmogorov-Smirnov distance metric to compare).

By construction, $q_{so90}$ values cannot exceed their corresponding $q_{sat}$ values, because the logit transformation maintains $RH_{ba}$ within its mathematical and physical limits [0, 100%]. The converse is however not true, as the logit transformation used to maintain $q_{ba}$ within its mathematical limits [0, 1] does not necessarily maintain it within its physical limits [0, $q_{sat}(T,P)$]. This is illustrated in Figure 5, which shows that supersaturation ($RH_{so90}$ > 100 %) is generated for all investigated adjustment techniques (results for Miami are representative of all study sites). Thus, after Figure 4 showed that preserving the relation $f(\cdot)$ or $g(\cdot)$ requires adjusting three of the involved variables and post-calculating the fourth one, Figure 5 shows that keeping all variables within meaningful bounds requires including RH within the three directly adjusted variables.

### 3.2. Intra-annual cycle

The effect of the adjustment techniques on the annual cycle is investigated by visual inspection of its general shape and of potential month-to-month jumps, a caveat already anticipated by Hewitson et al. (2014) and illustrated in Gennaretti et al. (2015). Figure 6 shows related results for the RH average annual cycle at one study site (Iqaluit) over 1981-2010, for the three temporal grouping options crossed with the three dimensionality options (with activated TP option; to which results are practically insensitive).

Using annual grouping (Figs. 6a, 6b and 6c) leads to unsatisfactory results regarding the general shape, as the transfer function ($F_{\mathrm{QM}}$) may link simulated and reference daily values from different moments of the year. However, Fig. 6b reveals that the shuffling process can take advantage of the respective intra-annual shapes of the master (here *T*) and the shuffled (here RH) variables to improve the general shape of the latter. With monthly grouping (Figs. 6d, 6e and 6f), the most striking problem is month-to-month jumps, particularly severe in Fig. 6d. Jumps stem from the fact that QM cannot adjust the ascending or descending character of intra-month sequences when the simulation and the reference product differ thereupon (see for June). Using a moving window (Figs. 6g, 6h and 6i) leaves results devoid of these two problems (bad cycle shape, and jumps). Qualitative conclusions for RH at Iqaluit are generally representative of those for other investigated variables and sites.

It is worth emphasizing that the month-to-month jumps stemming from the monthly temporal grouping of the days may easily go unnoticed when verifications are performed with monthly averages only. This is shown in Figure 7, where RH values (from Figs. 6d, 6e and 6f) are further averaged over the days of a same month; adjusted annual cycles look good from this perspective, which hides the intra-month ascending or descending prevalent character of the sequences.

### 3.3. Inter-annual variability

The effect of bias adjustment on inter-annual variability is investigated by calculating the standard deviation ($\sigma$) of the 30 intra-month averages over 1981-2010. Figure 8 shows this metric for each variable, for one study site (Denver), with window grouping and TP (results have rather weak sensitivity to these options). To estimate the natural variability envelop, the Matlab® *bootstrp*(·) function has been used to re-sample the 30 CFSR intra-month averages 10,000 times, and the 1$^{st}$ and 99$^{th}$ percentiles of resulting $\sigma$ values were retained (delimiting the grey boxes in Figure 8). Results illustrate that these techniques, operating on daily indices, do not necessarily adjust year-to-year variability, an effect already pointed out by Haerter et al. (2011) for a univariate technique. Biases in inter-annual variability are often reduced with QM-only and eig-QM, but there are cases of deterioration. For shuffled variables (*P*, *RH* and *q*) in QM-shuf, inter-annual variability is generally flattened (pushed towards zero), because time-exchange of daily elements involves above-average as well as below-average years. Among 1728 cases (12 sites x 12 months x 3 shuffled variables x 4 RCP8.5 simulations), $\sigma$ is found {above; within; below} the bootstrap envelop with respective frequencies of {22 %; 63 %; 15 %} with the raw simulation, {16 %; 77 %; 7 %} with QM-only, {4 %; 52 %; 43 %} with QM-shuf, and {16 %; 77 %; 7 %} with eig-QM (apparent differences from sums of 100 % are due to rounding). For the master variable (*T*) in QM-shuf, the small perceptible differences with QM-only (Fig. 8a) stem from the same-duration constraint for calibration/application periods with QM-shuf, which affects the regressions calculation.

### 3.4. Inter-variable correlation

The effect on inter-variable correlations has first been investigated by calculating the Spearman's (rank) correlation coefficients ($r_{rank}$) for all days in a same month-of-the-year over 1981-2010. Figure 9 shows the results for the pair of variables RH and *T*, for one study site (Mexico City), with monthly grouping and without TP (weak sensitivity to these options). Because in this case the metric is perfectly aligned with how the shuffling procedure works, Figure 9 is merely a verification that QM-shuf leads to a perfect match with CFSR. For eig-QM however, $r_{rank}$ values are not *a priori* expected to match perfectly with those of CFSR, as the procedure acts in a quadrivariate fashion (there is translation, rotation and resizing of the simulated point cloud, but no reshaping); results illustrate *a posteriori* that eig-QM generally results in a fair but imprecise adjustment for pairwise correlations.

Next, a comparison with an estimate of natural variability has been performed, which required modifying the verification metric. For each time series involved, the ensemble of the 30 intra-month $r_{rank}$ values was generated (e.g., $r_{rank}$ for the 31 days of May 1981, $r_{rank}$ for the 31 days of May 1982, and so on up to May 2010), and then the average of these 30 values calculated; analogously to the Section 3.3 situation, the bootstrap envelop is obtained by re-sampling 10,000 times among the 30 intra-month $r_{rank}$ values, and retaining the 1$^{st}$ and 99$^{th}$ percentiles of the resulting averages). Results are shown in Figure 10 for correlations between RH and each of the other variables, for one study site (Mexico City), with window grouping and TP activated (weak sensitivity to these options). For this example and this verification metric, large simulated biases are generally improved by multivariate procedures, but there are cases of deterioration for eig-QM (e.g., October on Fig. 10c). Among 3456 cases (12 sites x 12 months x 6 possible pairs of variables x 4 RCP8.5 simulations), the metric is found {above; within; below} the bootstrap envelop with respective frequencies of {29 %; 39 %; 33 %} with the raw simulation, {27 %; 40 %; 33 %} with QM-only, {13 %; 69 %; 18 %} with QM-shuf, and {11 %; 74 %; 15 %} with eig-QM (apparent differences from sums of 100 % are due to rounding).

3.5. Lag-1 auto-correlation

The effect on auto-correlation (AC) is investigated with the Spearman's (rank) correlation coefficient of lag 1. Calculations are performed analogously to those presented in Figure 10 for another property, with intra-month lag-1 AC calculated for each of the 30 instances of a given month-of-the-year over 1981-2010, and with the average subsequently taken. Figure 11 shows results for one site (El Paso), with window grouping and TP procedure (weak sensitivity to these options). Lag-1 AC values in raw simulations are roughly preserved by QM-only and eig-QM, whereas for shuffled variables (*P*, *RH* and *q*) in QM-shuf the values are pushed towards zero. Among 1728 cases (12 sites x 12 months x 3 shuffled variables x 4 RCP8.5 simulations), the metric is found {above; within; below} the bootstrap envelop with respective frequencies of {36 %; 50 %; 14 %} with the raw simulation, {34 %; 52 %; 14 %} with QM-only, {3 %; 10 %; 87 %} with QM-shuf, and {32 %; 55 %; 14 %} with eig-QM (apparent differences from sums of 100 % are due to rounding).

To further illustrate the effect of the shuffling on auto-correlation (AC), Figure 12 shows the RH time series for August 1981 at one site (El Paso), for raw and for adjusted SIM-01, with window grouping and TP activated. In this fairly representative example, the simulated 31-day segment presents a lag-1 AC value of 0.66, which changes to 0.64 with QM-only, to 0.01 with QM-shuf, and to 0.48 with eig-QM.

3.6. Climate change signals

The level of preservation of the simulated long-term changes is investigated with the so-called Δ (deltas) from 1981-2010 to 2071-2100. Figure 13 shows results for September $\Delta_{rel}(q_{ba})$ in function of corresponding $\Delta_{rel}(q_{sim})$ values, with the subscript 'rel' referring to relative changes. The justification for showing $\Delta_{rel}$ stems from recourse to the logit(·) transformation for *q*, which implicitly transfers the trend preservation (TP) effort from the absolute to the relative change; the situation is the same for RH, whereas for *T* and *P* it is the absolute changes that are tentatively preserved by the TP procedure. Figure 13 shows that $\Delta_{rel}(q_{sim})$ is often altered when TP is deactivated, a well-known general potential effect from quantile mapping. Activating TP generally leads to fair $\Delta_{rel}(q_{sim})$ preservation, with limitations for annual grouping and multivariate options (Figs. 13b and 13c) as the RMSD between $\Delta_{rel}(q_{ba})$ and $\Delta_{rel}(q_{sim})$ then does not decrease much (higher RMSD indicates higher discrepancy from the 1:1 ratio line).

A broader view of the results may be found in Figure 14, which presents the RMSD values for the study's main variables ($T_{ba}$, $P_{ba}$, $RH_{ba}$, $q_{ba}$, $RH_{so90}$, $q_{so90}$). Each panel has its own normalization, with all 216 RMSD values (12 months x 18 techniques) being divided by the maximum among these values. Results show that the most problematic no-TP situations (darker blue shades) are generally much improved by activating the TP procedure, except the striking case of $P_{ba}$ when shuffling allows inter-month exchanges (annual grouping). For RH, the TP procedure does not look effective, but this mostly reflects perturbations of RMSD values already small even without TP. For *q*, the panel essentially generalizes the September situation presented in Figure 13. No simple explanation has been found for why the problematic QM-shuf / annual grouping combination is pronounced for only one of the three shuffled variables; reasons possibly involve particularities in annual cycles of recent-past states and Δ's, as well as in Δ-to-σ (signal-to-noise) ratios. One interesting feature in Figure 14 is that the TP effect partly carries over to post-calculated $RH_{so90} \equiv f(T_{ba}, P_{ba}, q_{ba})$ and $q_{so90} \equiv g(T_{ba}, P_{ba}, RH_{ba})$ values, possibly due to a stabilizing effect from $T_{ba}$.

## 4. Summary with concluding remarks

The central objective of this study was to illustrate the distinction between two problems potentially involved in the statistical adjustment of climate simulations, namely multivariate biases and physical inconsistency. A multivariate bias problem occurs when a GCM or a RCM simulation presents inter-variable dependencies that are markedly different from those of a trusted reference (observation-based) product, if the research purpose requires these dependencies to be realistic. This potential problem concerns statistical properties that emerge over a very large number of time steps and from the model-as-a-whole (whose formulation is not in isomorphism with real-world physics), and here it has been monitored with pairwise correlations among temperature (*T*), pressure (*P*), specific humidity (*q*) and relative humidity (RH). A physical inconsistency problem occurs when a contradiction with a variable's definition or with a well-identified element of physics is generated. This potential problem concerns physics-based expectations at individual time steps, and here it has been monitored with the instantaneous thermodynamic relationship that links *T*, *P*, *q* and RH.

A supplementary objective was to help bias adjustment practitioners in identifying techniques that are adequate for specific research purposes; this was addressed by working with several typical procedures combined into 18 alternative techniques, and by investigating several statistical properties aside that involved in the central objective (inter-variable correlation). Main qualitative conclusions, based on 10 daily simulations at 12 sites across North America, are summarized in Table 3, where each row corresponds to the situation for either the raw simulation or one of the 18 bias adjustment techniques.

Regarding the thermodynamic relationship, results show that all investigated techniques break this instance of physical consistency when applied on simulations that are consistent thereupon (Figure 4). In particular, two procedures promoted to fix the multivariate bias problem, namely shuffling and eigenvector-based geometric transformations, have generated physical inconsistency, no matter the auxiliary decisions on trend preservation and on temporal grouping of the days. Of course there is an easy solution to this PI problem, which is to adjust only three of the variables and to post-calculate the fourth one, which amounts to explicitly considering the thermodynamic relationship in the bias adjustment strategy (note that RH shouldn't be the post-calculated variable; see Figure 5). In other words, a sophisticated bias adjustment technique may not be in itself a complete strategy, when the involved variables are constrained by a specific instantaneous physical link.

Note that this account opposes arguments from at least two widely held positions. The first position casts doubt upon legitimacy of bias adjustment in general, advancing as a main argument that it presumably destroys simulated physical consistency (e.g., Ehret et al., 2012; Chen et al. 2016; Sippel et al., 2016). Yet, as already stated, no model is *fully* or *holistically* consistent with physics, hence there is no such thing as an automatic destruction of physics as soon as a simulated emerging property is altered. Instead, a clear instance of contradiction with physics must be identified before raising the specter of physics destruction. And if a specific relationship can be pointed out, then it should be easy to incorporate it into the bias adjustment strategy. The second position promotes multivariate procedures, advancing inter alia the argument that mere univariate adjustment could lead to outputs with inappropriate physical laws or to inconsistency in underlying model physics (e.g., Cannon et al., 2015; François et al., 2020). Yet, this is based on a rather vague association between multivariate adjustment possibilities and model physics (or physics *tout court*). In fact, it is clear that any alteration to a simulation conceptually disconnects it from its generator (the model). But it is difficult to grasp why, in the particular case of multivariate statistical procedures, such disconnection would amount to a form of reconnection with the model physics formulation or with any specific physical law. Multivariate techniques add no physics to simulations, at least not in a reductionist way. And just like a good strategy involving a univariate technique may preserve a clear instance of physical consistency, a bad strategy involving a multivariate technique may destroy it.

One potential advantage of resorting to multivariate techniques is that, when a variable of interest is post-calculated to keep consistency with its directly-adjusted parent variables, its marginal residual biases could be lower if parent variables are adjusted in a multivariate way. Such advantage has been illustrated by Zscheischler et al. (2019) for the wet bulb globe temperature, a function of temperature and relative humidity. It must however be emphasized that in this case, it is not the involved multivariate technique (MBCn; Cannon, 2018) that brings instantaneous consistency between the variables; it is rather another piece of the adjustment strategy that plays this role, namely the explicit instruction to respect the function.

Regarding biases, Table 3 reveals an interesting portrait. Performing adjustment by grouping all days of the year may lead to unrealistic intra-annual cycles, and grouping them on a monthly basis may lead to important month-to-month jumps (Figure 6) that go unnoticed through monthly averages (Figure 7); such caveats are avoided when resorting to a moving window (Themeβl et al., 2012). Inter-annual variability is not directly targeted for adjustment by the techniques tested in this study, but *a posteriori* a prevalent improvement was found for QM-only and eig-QM alternatives. As for QM-shuf, the prevalent flattening effect expected *a priori* has been verified (Figure 8). Daily techniques could eventually be subsumed into the cascade approach proposed by Haerter et al. (2011), which also favors adjustment of inter-annual intra-month averages. Inter-variable correlation is the hallmark of bivariate QM-shuf (Figure 9), whereas QM-only essentially keeps the simulated values and quadrivariate eig-QM is shown *a posteriori* to have a prevalent improvement effect (Figure 10; for these results it must be recalled that the verification metric is de-aligned from the exact way the shuffling operates). Finally, simulated auto-correlation was essentially kept by QM-only and eig-QM alternatives (Figure 11). In contrast, QM-shuf has a prevalent suppressing effect on auto-correlation (except for the master variable), which is well illustrated by day-to-day sequences (Figure 12). The TP optional procedure generally had a weak effect on the calibration period's biases situation, and its general ability to preserve simulated monthly changes (Δ) can fairly be granted except when combining QM-shuf or eig-QM with annual grouping (Figures 13 and 14). Note that there exists a defendable position emphasizing that signal alteration is just a normal consequence of the quantile-dependent character of the bias (e.g., Gobiet et al., 2015).

This study was not intended to bring out any better bias adjustment technique. Instead, Table 3 should be viewed as a helpful chart matching several potential choices with likely effects on the input simulations. Assuming a preceding careful simulation selection step, this is in line with adequacy-for-purpose thinking (Parker, 2009; Parker, 2020), because procedures are not viewed as valid or not, but rather as adequate or not in a given context of use. This however does not hinder the identification of particular difficulties for certain procedures. For example, shuffling does not look good in the context of bias adjustment. Indeed, for the benefit of adjusting inter-variable correlations, it flattens inter-annual variability and suppresses auto-correlation, two properties for which climate models often have an interesting level of success (e.g., Figures 8 and 11). Moreover, resorting to shuffling limits the application period to the same duration as that of the calibration period, unless one works with multiple blocks (with conceivable period-to-period jumps, an issue however not investigated in this study). But the most particular difficulty is arguably that shuffling does not allow inter-variable correlations to evolve over time, at least not as used in the $R^2D^2$ technique (Vrac, 2018) whereas the situation thereupon is unclear for the MBCn technique (François et al., 2020). This is paradoxical for future climate change studies, as inter-variable correlations are thus considered important enough to be adjusted, but not important enough to retain an eventual simulated evolution in this property. Nevertheless, *a priori* it cannot be ruled out that shuffling be an adequate procedure for specific end-user purposes.

Finally, it must be mentioned that the covering of multivariate procedures in this study is not exhaustive. For example, the dOTC technique recently proposed by Robin et al. (2019) and which extends the QM concept to more than one dimension by minimizing a cost function, was not included. Idem for the MBCn technique of Cannon (2018), which combines random geometric rotations and back rotations, a QM variant and a final shuffling step. Including them would not have changed the way to illustrate the distinction between the notions of multivariate bias and physical inconsistency, but it would be interesting to investigate whether these techniques can preserve the $T$-$P$-RH-$q$ thermodynamic relationship without being explicitly instructed to. Also, this study does not have the conceptual scope covered by Maraun et al. (2017), who advocate for a process-based orientation of bias adjustment.

Indeed, dynamic meteorological processes are more complex than instantaneous relationships, lying somewhere between basic prescribed physics elements and long-term emerging properties.

**Acknowledgements**

We acknowledge the World Climate Research Programme's Working Group on Coupled Modelling, which is responsible for CMIP, and thank the climate modelling institutes (listed in Table 1 of this paper) for producing and making their model outputs available. The U.S. Department of Energy's Program for Climate Model Diagnosis and Intercomparison provides coordinating support and leads the development of software infrastructure for CMIP in partnership with the Global Organization for Earth System Science Portals. The CRCM5 simulation has been generated and supplied by Ouranos. We also thank the Climate Forecast System Reanalysis (CFSR) team for making its reanalysis product publicly available. A Master's fellowship from Ouranos and the Mitacs Accelerate program made this study possible. Finally, we would like to thank Prof. René Laprise (UQAM) for valuable comments on the manuscript.

## Appendix A - List of acronyms

| | |
|---|---|
| AC | auto-correlation |
| CFSR | Climate Forecast System Reanalysis |
| CMIP5 | Coupled Model Intercomparison Project - phase 5 |
| CRCM5 | Canadian Regional Climate Model - version 5 |
| dOTC | Dynamical Optimal Transport Correction (algorithm) |
| GCM | global climate model |
| MBCn | Multivariate Bias Correction with *N*-dimensional transform (algorithm) |
| PI | physical inconsistency |
| QM | quantile mapping |
| RCM | regional climate model |
| RCP | Representative Concentration Pathways |
| $R^2D^2$ | Rank Resampling for Distributions and Dependences (algorithm) |
| RH | relative humidity |
| RMSD | root-mean-square difference |
| RMSE | root-mean-square error |
| SIM-*x* | simulation number *x* |
| TP | trend preservation |
| UTC | Universal Time Coordinated |
| WMO | World Meteorological Organization |

## List of references

Addor N. and Fischer E. M. (2015). The influence of natural variability and interpolation errors on bias characterization in RCM simulations. *Journal of Geophysical Research: Atmospheres*, 120 (19), p. 10180-10195, doi: 10.1002/2014JD022824.

Agbazo M. N. and Grenier P. (2019). Characterizing and avoiding physical inconsistency generated by the application of univariate quantile mapping on daily minimum and maximum temperatures over Hudson Bay. *International Journal of Climatology*, 40 (8), p. 3868-3884, doi: 10.1002/joc.6432.

Arora V. K. and Coauthors (2011). Carbon emission limits required to satisfy future representative concentration pathways of greenhouse gases. *Geophysical Research Letters*, 38 (5), doi: 10.1029/2010GL046270.

Cannon A. J., Sobie S. R. and Murdock T. Q. (2015). Bias Correction of GCM Precipitation by Quantile Mapping: How Well Do Methods Preserve Changes in Quantiles and Extremes? *Journal of Climate*, 28 (17), p. 6938-6959, doi: 10.1175/JCLI-D-14-00754.1.

Cannon A. J. (2018). Multivariate quantile mapping bias correction: An *N*-dimensional probability density function transform for climate model simulations of multiple variables. *Climate dynamics*, 50 (1), p. 31-49, doi: 10.1007/s00382-017-3580-6.

Chen J., Gauvin St-Denis B., Brissette F. and Lucas-Picher P. (2016). Using Natural Variability as a Baseline to Evaluate the Performance of Bias Correction Methods in Hydrological Climate Change Impact Studies. *Journal of Hydrometeorology*, 17 (8), p. 2155-2174, doi: 10.1175/JHM-D-15-0099.1.

Cleveland W. S. (1979). Robust Locally Weighted Regression and Smoothing Scatterplots. *Journal of the American Statistical Association*, 74 (368), p. 829-836.

Del Genio A.D., Yao M.-S., Kovari W. and Lo K. K.-W. (1996). A prognostic cloud water parameterization for global climate models. *Journal of Climate*, 9 (2), p. 270-304, doi: 10.1175/1520-0442(1996)009<0270:APCWPF>2.0.CO:2.

Diaconescu E. P., Mailhot A., Brown R. and Chaumont D. (2017). Evaluation of CORDEX-Arctic daily precipitation and temperature-based climate indices over Canadian Arctic land areas. *Climate Dynamics*, 50 (5), p. 2061-2085, doi: 10.1007/s00382-017-3736-4.

Dunne J.P. and Coauthors (2012). GFDL's ESM2 global coupled climate–carbon earth system models. Part I: Physical formulation and baseline simulation characteristics. *Journal of Climate*, 25 (19), p. 6646-6665, doi: 10.1175/JCLI-D-11-00560.1.

Ehret U., Zehe E., Wulfmeyer V., Warrach-Sagi K. and Liebert J. (2012). Should we apply bias correction to global and regional climate model data? *Hydrology and Earth System Sciences*, 16 (9), p. 3391-3404, doi: 10.5194/hess-16-3391-2012.

Findlater K., Webber S., Kandlikar M. and Donner S. (2021). Climate services promise better decisions but mainly focus on better data. *Nature Climate Change*, 11, p. 731-737, doi: 10.1038/s41558-021-01125-3.

Flato G. and Coauthors (2013). Evaluation of climate models. In *Climate Change 2013: The Physical Science Basis. Contribution of Working Group I to the Fifth Assessment Report of the Intergovernmental Panel on Climate Change, Cambridge University Press,* p. 741-882, doi: 10.1017/CBO9781107415324.020.

François B., Vrac M., Cannon A. J., Robin Y. and Allard D. (2020). Multivariate bias corrections of climate simulations: which benefits for which losses? *Earth System Dynamics*, 11 (2), p. 537-562, doi: 10.5194/esd-11-537-2020.

Gennaretti F., Sangelantoni L. and Grenier P. (2015). Toward daily climate scenarios for Canadian Arctic coastal zones with more realistic temperature-precipitation interdependence. *Journal of Geophysical Research: Atmospheres*, 120 (23), p. 11862-11877, doi: 10.1002/2015JD023890.

Giere R. N. (2010). An agent-based conception of models and scientific representation. *Synthese*, 172 (2), p. 269-281, doi: 10.1007/s11229-009-9506-z.

Gobiet A., Suklitsch M. and Heinrich G. (2015). The effect of empirical-statistical correction of intensity-dependent model errors on the temperature climate change signal. *Hydrology and Earth System Sciences*, 19 (10), p. 4055-4066, doi: 10.5194/hess-19-4055-2015.

Gómez-Navarro J. J., Raible C. C., Bozhinova D., Martius O., García Valero J. A. and Montávez J. P. (2018). A new region-aware bias-correction method for simulated precipitation in areas of complex orography. *Geoscientific Model Development*, 11 (6), p. 2231-2247, doi: 10.5194/gmd-11-2231-2018.

Grenier P. (2018). Two types of physical inconsistency to avoid with univariate quantile mapping: a case study over North America concerning relative humidity and its parent variables. *Journal of Applied Meteorology and Climatology*. 57 (2), p. 347-364, doi: 10.1175/JAMC-D-17-0177.1.

Haerter J. O., Hagemann S., Moseley C. and Piani C. (2011). Climate model bias correction and the role of timescales. *Hydrology and Earth System Sciences*, 15 (3), p. 1065-1079, doi: 10.5194/hess-15-1065-2011.

Hecht A. D. (1984). Meeting the challenge of climate service in the 1980s. *Bulletin of the American Meteorological Society*, 65 (4), p. 365-366, doi: 10.1175/1520-0477(1984)065<0365:MTCOCS>2.0.CO:2.

Hempel S., Frieler K., Warszawski L., Schewe J. and Piontek F. (2013). A trend-preserving bias correction - the ISI-MIP approach. *Earth System Dynamics*, 4 (2), p. 219-236, doi: 10.5194/esd-4-219-2013.

Hewitson B. C., Daron J., Crane R. G., Zermoglio M. F. and Jack C. (2014). Interrogating empirical-statistical downscaling. *Climatic Change*, 122 (4), p. 539-554, doi: 10.1007/s10584-013-1021-z.

Hewitt C. D. and Coauthors (2021). Recommendations for Future Research Priorities for Climate Modeling and Climate Services. *Bulletin of the American Meteorological Society*, 102 (3), p. E578-E588, doi: 10.1175/BAMS-D-20-0103.1.

Hnilica J., Hanel M. and Puš V. (2017). Multisite bias correction of precipitation data from regional climate models. *International Journal of Climatology*, 37 (6), p. 2934-2946, doi: 10.1002/joc.4890.

Jacobson M. Z. (2005). Fundamentals of atmospheric modelling (Second Edition). *Cambridge University Press*.

Kotlarski S. and Coauthors (2019). Observational uncertainty and regional climate model evaluation: A pan-European perspective. *International Journal of Climatology*, 39 (9), p. 3730-3749, doi: 10.1002/joc.5249.

Kuhn T. (1977). Objectivity, value judgment, and theory choice. In *The Essential Tension: Selected studies in scientific tradition and change*, *University of Chicago press*, p. 320-339.

Lanzante J. R., Dixon K. W., Nath M. J., Whitlock J. E. and Adams-Smith D. (2018). Some pitfalls in statistical downscaling of future climate. *Bulletin of the American Meteorological Society*, 99 (4), p. 791-803, doi: 10.1175/BAMS-D-17-0046.1.

Laprise R. (2008). Regional climate modelling. *Journal of Computational Physics*, 227 (7), p. 3641-3666, doi: 10.1016/j.jcp.2006.10.024.

Laudan L. (1984). Kuhn's critique of methodology. In: *Science and values: The aims of science and their role in scientific debate*, *University of California Press*, p. 87-102.

Lehtonen I., Kämäräinen M., Gregow H., Venäläinen A. and Peltola H. (2016). Heavy snow loads in Finnish forests respond regionally asymmetrically to projected climate change. *Natural Hazards and Earth System Sciences*, 16 (10), p. 2259-2271, doi: 10.5194/nhess-16-2259-2016.

Lenhard J. and Winsberg E. (2010). Holism, Entrenchment, and the Future of Climate Model Pluralism. *Studies in History and Philosophy of Science*, 41 (3), p. 253-262, doi: 10.1016/j.shpsb.2010.07.001.

Lourenço T., Swart R., Goosen H. and Street R. (2016). The rise of demand-driven climate services. *Nature Climate Change*, 6 (1), p. 13-14, doi: 10.1038/nclimate2836.

Lugen M. (2020). Framing Climate Services: Logics, Actors, and Implications for Policies and Projects. *Atmosphere*, 11 (10), p. 1047, doi: 10.3390/atmos11101047.

Maraun D. and Coauthors (2017). Towards process-informed bias correction of climate change simulations. *Nature Climate Change*, 7 (11), p. 764-773, doi: 10.1038/nclimate3418.

Martins J., Fraga H., Fonseca A. and Santos J. A. (2021). Climate Projections for Precipitation and Temperature Indicators in the Douro Wine Region: The Importance of Bias Correction. *Agronomy*, 11 (5), p. 990, doi: 10.3390/agronomy11050990.

Parker W. S. (2009). Confirmation and Adequacy-for-Purpose in Climate Modeling. *Proceedings of the Aristotelian Society*, Supplementary Volume 83 (1), p. 233-249, doi: 10.1111/j.1467-8349.2009.00180.x.

Parker W. S. (2020). Model Evaluation: An Adequacy-for-Purpose View. *Philosophy of Science*, 87 (3), p. 457-477, doi: 10.1086/708691.

Peel M. C., Finlayson B. L. and McMahon T. A. (2007). Updated world map of the Köppen-Geiger climate classification. *Hydrology and Earth System Sciences*, 11 (5), p. 1633-1644, doi: 10.5194/hess-11-1633-2007.

Petersen A. C. (2000). Philosophy of climate science. *Bulletin of the American Meteorological Society*, *81* (2), p. 265-272, doi: 10.1175/1520-0477(2000)081<0265:POCS>2.3.CO;2.

Piani C. and Haerter J. O. (2012). Two dimensional bias correction of temperature and precipitation copulas in climate models. *Geophysical Research Letters*, 39 (20), doi: 10.1029/2012GL053839.

Pruppacher H. R. and Klett J. D. (1997). Microphysics of clouds and precipitation (Second Edition). *Kluwer academic Publishers*, p. 954.

Robin Y., Vrac M., Naveau P. and Yiou P. (2019). Multivariate stochastic bias corrections with optimal transport. *Hydrology and Earth System Sciences*, 23 (2), p. 773-786, doi: 10.5194/hess-23-773-2019.

Ruosteenoja K., Jylhä K., Räisänen J. and Mäkelä A. (2017). Surface air relative humidities spuriously exceeding 100% in CMIP5 model output and their impact on future projections. *Journal of Geophysical Research: Atmospheres*, 122 (18), p. 9557-9568, doi: 10.1002/2017JD026909.

Saha S. and Coauthors (2010). The NCEP Climate Forecast System Reanalysis. *Bulletin of the American Meteorological Society*, 91 (8), p. 1015-1058, doi: 10.1175/2010BAMS3001.1.

Šeparović L., Alexandru A., Laprise R., Martynov A., Sushama L., Winger K., Tete K. and Valin M. (2013). Present climate and climate change over North America as simulated by the fifth-generation Canadian regional climate model. *Climate Dynamics*, 41 (11), p. 3167-3201, doi: 10.1007/s00382-013-1737-5.

Sippel S., Otto F. E. L., Forkel M., Allen M. R., Guillod B. P., Heimann M., Reichstein M., Seneviratne S. I., Thonicke K. and Mahecha D. (2016). A novel bias correction methodology for climate impact simulations. *Earth System Dynamics*, 7 (1), p. 71-88, doi: 10.5194/esd-7-71-2016.

Sonntag D. (1990). Important new values of the physical constants of 1986, vapor pressure formulations based on ITS-90 and psychrometer formulae. *Zeitschrift für Meteorologie*, 40 (5), p. 340-344.

Steel D. (2010). Epistemic values and the argument from inductive risk. *Philosophy of Science*, 77 (1), p. 14-34, doi: 10.1086/650206.

Su T., Chen J., Cannon A. J., Xie P. and Guo Q. (2020). Multi-site bias correction of climate model outputs for hydro-meteorological impact studies: An application over a watershed in China. *Hydrological Processes*, 34 (11), p. 2575-2598, doi: 10.1002/hyp.13750.

Taylor K. E., Stouffer R. J. and Meehl G. A. (2012). An Overview of CMIP5 and the Experiment Design. *Bulletin of the American Meteorological Society*, 93 (4), p. 485-498, doi: 10.1175/BAMS-D-11-00094.1.

Themeßl M. J., Gobiet A. and Heinrich G. (2012). Empirical-statistical downscaling and error correction of regional climate models and its impact on the climate change signal. *Climatic Change*, 112 (2), p. 449-468, doi: 10.1007/s10584-011-0224-4.

Thrasher B., Maurer E. P., McKellar C. and Duffy P. B. (2012). Technical Note: Bias correcting climate model simulated daily temperature extremes with quantile mapping. *Hydrology and Earth System Sciences*, 16 (9), p. 3309-3314, doi: 10.5194/hess-16-3309-2012.

Vrac M. and Friederichs P. (2015). Multivariate - Intervariable, Spatial, and Temporal - Bias Correction. *Journal of Climate*, 28 (1), p. 218-237, doi: 10.1175/JCLI-D-14-00059.1.

Vrac M. (2018). Multivariate bias adjustment of high-dimensional climate simulations: the Rank Resampling for Distributions and Dependences ($R^2D^2$) bias correction. *Hydrology and Earth System Sciences*, 22 (6), p. 3175-3196, doi: 10.5194/hess-22-3175-2018.

Wallace J. M. and Hobbes P. V. (2006). Atmospheric Science: An introductory Survey (Second Edition). *Elsevier Academic Press*, 92, p. 483.

Watanabe M. and Coauthors (2010). Improved Climate Simulation by MIROC5: Mean States, variability, and Climate Sensitivity. *Journal of Climate*, 23 (23), p. 6312-6335, doi: 10.1175/2010JCLI3679.1.

Wilcke R. A. I., Mendlik T. and Gobiet A. (2013). Multi-variable error correction of regional climate models. *Climatic Change*, 120 (4), p. 871-887, doi: 10.1007/s10584-013-0845-x.

Winsberg E. (2018). Philosophy and climate science. *Cambridge University Press*, doi: 10.1017/9781108164290.

Yukimoto S. and Coauthors (2012). A New Global Climate Model of the Meteorological Research Institute: MRI-CGCM3 - Model Description and Basic Performance. *Journal of the Meteorological Society of Japan*, 90, p. 23-64, doi: 10.2151/jmsj.2012-A02.

Zscheischler J., Fischer E. M. and Lange S. (2019). The effect of univariate bias adjustment on multivariate hazard estimates. *Earth System Dynamics*, 10 (1), p. 31-43, doi: 10.5194/esd-10-31-2019.

## Tables

Table 1: Specifications for simulations used in this study. Expansions for names of modelling institutes and models can be found at http://www.ametsoc.org/PubsAcronymList.

| Code for present study | Modelling institute | Model | Emission scenario | Member | Spatial resolution (latitude x longitude) | Reference |
|---|---|---|---|---|---|---|
| SIM-01 | MIROC | MIROC5 | RCP 2.6 | r1i1p1 | 1.4008 ° x 1.4062 ° | Watanabe et al. (2010) |
| SIM-02 | MIROC | MIROC5 | RCP 4.5 | r1i1p1 | 1.4008 ° x 1.4062 ° | |
| SIM-03 | MIROC | MIROC5 | RCP 6.0 | r1i1p1 | 1.4008 ° x 1.4062 ° | |
| SIM-04 | MIROC | MIROC5 | RCP 8.5 | r1i1p1 | 1.4008 ° x 1.4062 ° | |
| SIM-05 | MRI | MRI-CGCM3 | RCP 2.6 | r1i1p1 | 1.1215 ° x 1.1250 ° | Yukimoto et al. (2012) |
| SIM-06 | MRI | MRI-CGCM3 | RCP 4.5 | r1i1p1 | 1.1215 ° x 1.1250 ° | |
| SIM-07 | MRI | MRI-CGCM3 | RCP 6.0 | r1i1p1 | 1.1215 ° x 1.1250 ° | |
| SIM-08 | MRI | MRI-CGCM3 | RCP 8.5 | r1i1p1 | 1.1215 ° x 1.1250 ° | |
| SIM-09 | NOAA-GFDL | GFDL-ESM2G | RCP 8.5 | r1i1p1 | 2.0225 ° x 2.5000 ° | Dunne et al. (2012) |
| SIM-10* | Ouranos | CanESM2 / CRCM5 | RCP 8.5 | r2i1p1 | 0.22° ** | Šeparović et al. (2013) Arora et al. (2011) |

* This is the only regional simulation of the ensemble; Ouranos internal identification code is bbi/bbh.

** The CRCM5 grid is rotated relative to meridians and parallels.

Table 2: Specifications for study sites.

| Site | WMO station ID | Latitude of station (ºN) | Longitude of station (ºW) | Altitude of station (m) | Altitude of CFSR nearest grid tile (m) |
|---|---|---|---|---|---|
| Miami | 72202 | 25.8 | 80.4 | 5 | 1 |
| El Paso | 72270 | 31.8 | 106.4 | 1197 | 1314 |
| Denver | 72565 | 39.9 | 104.7 | 1640 | 1512 |
| San Francisco | 72494 | 37.6 | 122.4 | 3 | 62 |
| Mexico City | 76679 | 19.4 | 99.1 | 2235 | 2571 |
| New Orleans | 72231 | 30.0 | 90.3 | 5 | -3 |
| Vancouver | 71892 | 49.2 | 123.2 | 4 | 56 |
| St-Louis | 72434 | 38.8 | 90.4 | 171 | 158 |
| Montreal | 71627 | 45.5 | 73.7 | 36 | 10 |
| St-John's | 71801 | 47.6 | 52.7 | 141 | 30 |
| Yellowknife | 71936 | 62.5 | 114.4 | 206 | 225 |
| Iqaluit | 71909 | 63.8 | 68.6 | 34 | 258 |

Table 3: Synthesis of bias adjustment effects on simulated time series properties for each alternative technique, which is a combination of a dimensionality option (QM-only, QM-shuf or eig-QM), a temporal grouping option (annual, monthly or window), and an optional trend preservation procedure that is activated (TP) or not (-). For the PI problem: dark green indicates respect of the thermodynamic constraint (no PI); and dark red indicates a quasi-guaranteed breaking. For biases: grey indicates that simulated results are roughly kept; dark green stands for realistic results also expected *a priori*; light green for prevalent improvement noticed *a posteriori*; light red for prevalent deterioration noticed *a posteriori*; and dark red for clear deterioration also expected *a priori*. For long-term changes: grey indicates that simulated changes are roughly kept; and light red stands for frequent strong alteration noticed *a posteriori*. Note that for QM-shuf combinations, some red cases concern only the shuffled variables (here $P_{ba}$, $RH_{ba}$ and $q_{ba}$), whereas results for the master variable (here $T_{ba}$) are in line with the corresponding QM-only results.

| bias adjustment technique | | | instantaneous thermodynamic consistency ($q_{ba} = q_{so90}$) | biases | | | | | monthly long-term changes |
|---|---|---|---|---|---|---|---|---|---|
| | | | | intra-annual cycle | | monthly verification metrics | | | |
| | | | | shape | jumps | inter-annual variability | inter-variable correlation | lag-1 auto-correlation | |
| raw simulation | | | | | | | | | |
| QM-only | annual | TP | | | | | | | |
| | | - | | | | | | | |
| | monthly | TP | | | | | | | |
| | | - | | | | | | | |
| | window | TP | | | | | | | |
| | | - | | | | | | | |
| QM-shuf | annual | TP | The problem can be solved by explicitly considering the thermodynamic relationship within the bias adjustment strategy. | | | shuffled | | shuffled | shuffled |
| | | - | | | | shuffled | | shuffled | |
| | monthly | TP | | | | shuffled | | shuffled | |
| | | - | | | | shuffled | | shuffled | |
| | window | TP | | | | shuffled | | shuffled | |
| | | - | | | | shuffled | | shuffled | |
| eig-QM | annual | TP | | | | | | | |
| | | - | | | | | | | |
| | monthly | TP | | | | | | | |
| | | - | | | | | | | |
| | window | TP | | | | | | | |
| | | - | | | | | | | |

**Figure captions**

Figure 1: Diagram of the connections between the raw simulated (with subscripts 'sim') and the bias-adjusted (with either 'uni' or 'multi' subscripts, referred to by the more general 'ba' subscript elsewhere) variables. The role of the corresponding CFSR variables is implicit in this diagram. The variable $q_{\mathrm{so90}}$ is post-calculated to be consistent with $T_{\mathrm{ba}}$, $P_{\mathrm{ba}}$ and $\mathrm{RH}_{\mathrm{ba}}$.

Figure 2: Diagram of the bias adjustment algorithm used in this study, showing the place of each of the optional decisions.

Figure 3: General diagram of the variables' categorization and transformations necessary to prevent bias adjustment from generating physical inconsistency of the out-of-bound type. Vertical blue bands represent the potential extension of the empirical distribution. Here variables are referred to by their conventional GCM or RCM labels, and variables used in this study are highlighted in red ('tas' for *T*, 'ps' for *P*, 'huss' for *q*, and 'hurs' for *RH*).

Figure 4: Two-dimensional counts for $q_{ba}$ and $q_{so90}$, for one study site (Montreal) and for 9 of the 18 alternative adjustment techniques (TP option is activated). Counts include the ten simulations over the full application period (1981-2100), for a total of 438,000 time steps. Bin size is 0.25 g/kg x 0.25 g/kg. Black lines indicate the 1:1 ratio. On each panel, the root-mean-square error (RMSE) between $q_{ba}$ and $q_{so90}$ is provided as a numerical indication of physical inconsistency (departure from the 1:1 ratio).

Figure 5: Frequency (per mil) and amplitude (%) of supersaturation (SS) occurrences in $\mathrm{RH}_{\mathrm{so90}}$, for one study site (Miami) and for each of the 18 bias adjustment techniques. Each distribution is built from the SS cases among 438,000 considered time steps (10 simulations over the application period 1981-2100), with the solid line positioned at the SS frequency (*x* axis) and extending over the full range of obtained SS amplitudes (along the *y* axis), and the empty (or filled) circle representing the 50$^{\mathrm{th}}$ (or 90$^{\mathrm{th}}$) percentile. Lowercase (or uppercase) letters are used to represent the deactivated (or activated) TP option, and the matching regarding the dimensionality and grouping options is the following: a/A for QM-only and annual; b/B for QM-shuf and annual; c/C for eig-QM and annual; d/D for QM-only and monthly; e/E for

QM-shuf and monthly; f/F for eig-QM and monthly; g/G for QM-only and window; h/H for QM-shuf and window; i/I for eig-QM and monthly.

Figure 6: RH average annual cycle over the calibration period (1981-2010), for one study site (Iqaluit) and for 9 of the 18 alternative adjustment techniques (TP option is activated). The black line (corresponding to the reference product CFSR) and the red lines (each corresponding to one of the 10 raw simulations) are the same for all panels. Each blue line is the adjusted version of a raw simulation. Tick marks of the *x* axis indicate the first day of each month.

Figure 7: RH monthly average over the calibration period (1981-2010), for one study site (Iqaluit), for raw simulations (red), adjustment with QM-only (blue), adjustment with QM-shuf (green) and adjustment with eig-QM (purple). Each circle indicates one of the 10 (raw or adjusted) simulations (with superimposition in adjustment cases). Monthly grouping and TP options are activated. Black lines represent RH monthly averages for the reference product CFSR.

Figure 8: Standard deviation (σ) of monthly averages over the calibration period (1981-2010), for one study site (Denver), for variables: a) *T*; b) *P*; c) RH; and d) *q*. Each circle indicates one of the 10 (raw or adjusted) simulations, with same color code as in Figure 7. Window grouping and TP options are activated. Black lines represent CFSR σ values, and grey boxes delimit the 1$^{st}$ and 99$^{th}$ percentiles from 10,000 bootstrapping re-samplings of the 30 CFSR monthly averages.

Figure 9: Spearman's (rank) correlation coefficient ($r_{rank}$) between RH and *T*, for all days in each month-of-the-year over the calibration period (1981-2010), for one study site (Mexico City). Each circle indicates one of the 10 (raw or adjusted) simulations, with same color code as in Figure 7. Window grouping is activated and TP is deactivated. Black lines represent CFSR $r_{rank}$ values.

Figure 10: Average of the 30 intra-month $r_{rank}$ values over the calibration period (1981-2010), for one study site (Mexico City), for pairs of variables: a) RH and *T*; b) RH and *P*; and c) RH and *q*. Each circle indicates one of the 10 (raw or adjusted) simulations, with same color code as in Figure 7. Window grouping and TP options are activated. Black lines represent CFSR average intra-month $r_{rank}$ values, and

grey boxes delimit the 1st and 99th percentiles from 10,000 bootstrapping re-samplings of the 30 CFSR intra-month $r_{rank}$ values.

Figure 11: Average of the 30 intra-month lag-1 auto-correlation (AC) values over the calibration period (1981-2010), for one study site (El Paso), for: a) $T$; b) $P$; c) RH; and d) $q$. Each circle indicates one of the 10 (raw or adjusted) simulations, with same color code as in Figure 7. Window grouping and TP options are activated. Black lines represent CFSR average intra-month lag-1 AC values, and grey boxes delimit the 1st and 99th percentiles from 10,000 bootstrapping re-samplings of the 30 CFSR intra-month lag-1 AC values.

Figure 12: RH time series (at 12 UTC each day) for August 1981 at one site (El Paso), for raw SIM-01 and after different adjustments (window grouping and TP options activated in each case).

Figure 13: Relative long-term changes for September average specific humidity after adjustment, $\Delta_{rel}(q_{ba})$, in function of corresponding simulated changes, $\Delta_{rel}(q_{sim})$. Each panel contains 120 red symbols for adjustment with activated TP, and 120 blue symbols for adjustment without this procedure (12 sites x 10 simulations). Relative changes follow the general form [$\Delta_{rel}(q) \equiv 100(q(2071\text{-}2100) - q(1981\text{-}2010)) / q(1981\text{-}2010)$], in units of [% (90 yr)$^{-1}$]. Black lines indicate the 1:1 proportion, and printed root-mean-square differences (RMSD) are calculated over pairs of corresponding $\Delta_{rel}(q_{ba})$ and $\Delta_{rel}(q_{sim})$ values.

Figure 14: Root-mean-square differences (RMSD) over 120 pairs of corresponding bias-adjusted and raw simulated 1981-2010-to-2071-2100 change ($\Delta$ or $\Delta_{rel}$) values (12 sites x 10 simulations), for variables a) $T_{ba}$; b) $P_{ba}$; c) $RH_{ba}$; d) $q_{ba}$; e) $RH_{so90}$; and f) $q_{so90}$; and for all months (panel columns) and techniques (panel rows). Blue-shade upper-left (or red-shade lower-right) triangles correspond to technique without (or with) the trend preservation (TP) procedure. Labels ‘a’, ‘m’ and ‘w’ refer to annual, monthly and window grouping options, respectively. For each panel, RMSD values are presented as the fraction (white for 0 to 0.1, darker shade for 0.9 to 1) of the maximum of the 240 involved values. An empty (or filled) black dot indicates the associated with-TP RMSD value is larger than half its corresponding no-TP value (or larger than the corresponding no-TP value).

**Figures**

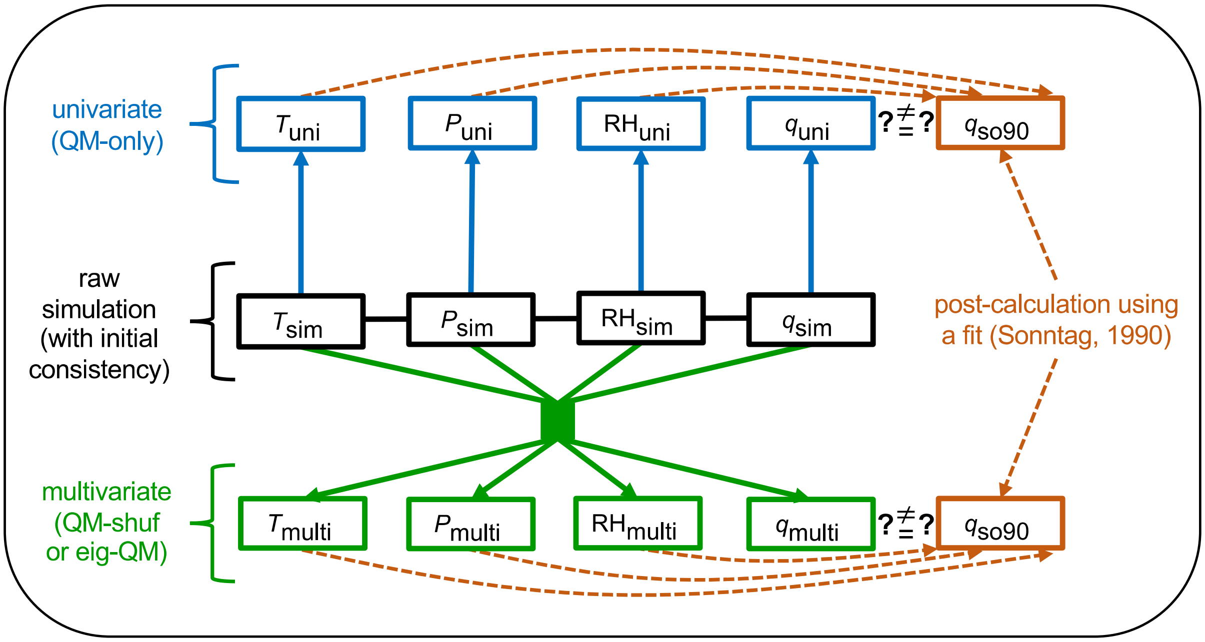


Figure 1: Diagram of the connections between the raw simulated (with subscripts 'sim') and the bias-adjusted (with either 'uni' or 'multi' subscripts, referred to by the more general 'ba' subscript elsewhere) variables. The role of the corresponding CFSR variables is implicit in this diagram. The variable $q_{so90}$ is post-calculated to be consistent with $T_{ba}$, $P_{ba}$ and $RH_{ba}$.

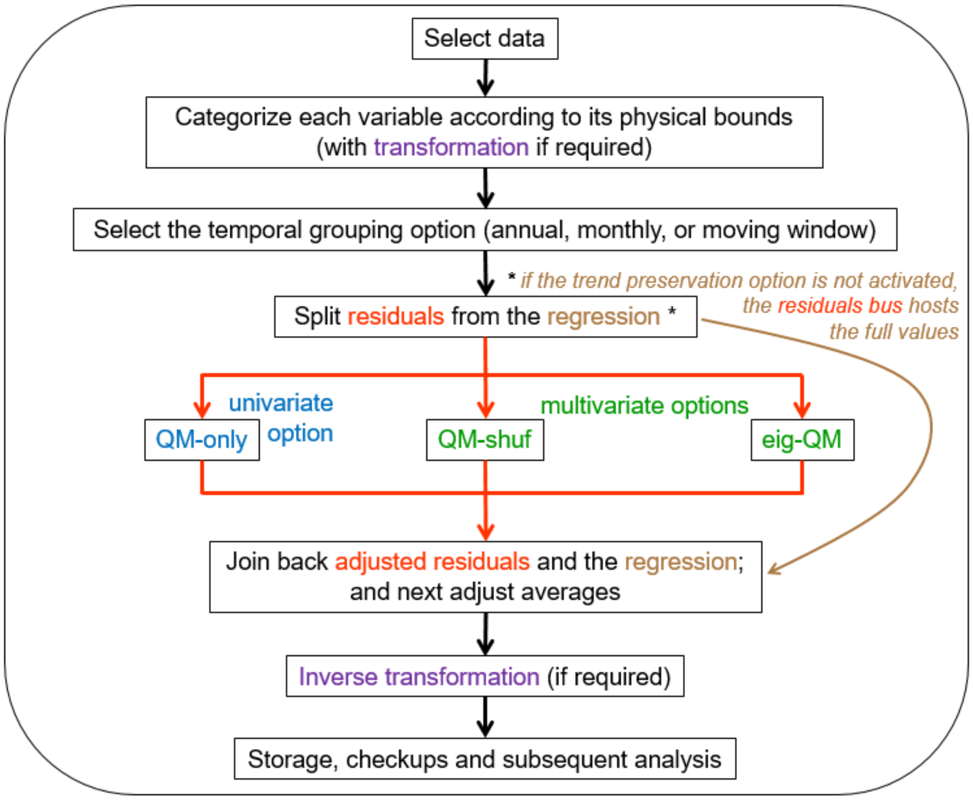


Figure 2: Diagram of the bias adjustment algorithm used in this study, showing the place of each of the optional decisions.

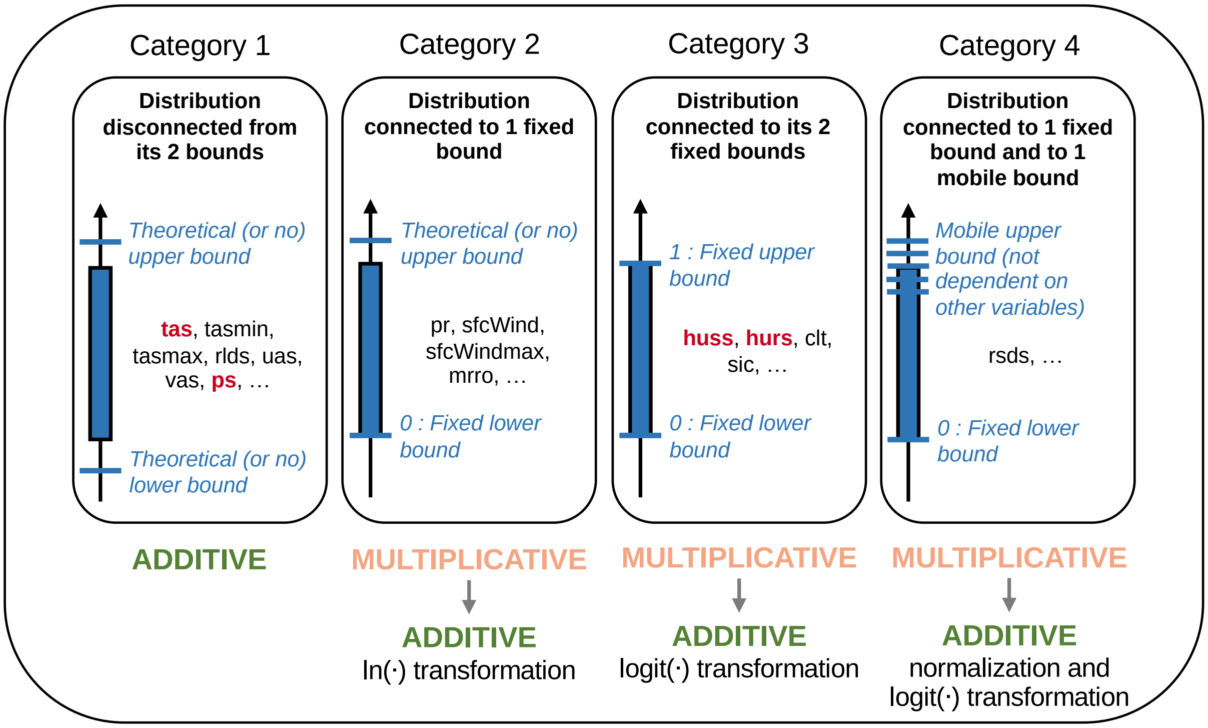


Figure 3: General diagram of the variables' categorization and transformations necessary to prevent bias adjustment from generating physical inconsistency of the out-of-bound type. Vertical blue bands represent the potential extension of the empirical distribution. Here variables are referred to by their conventional GCM or RCM labels, and variables used in this study are highlighted in red ('tas' for *T*, 'ps' for *P*, 'huss' for *q*, and 'hurs' for *RH*).

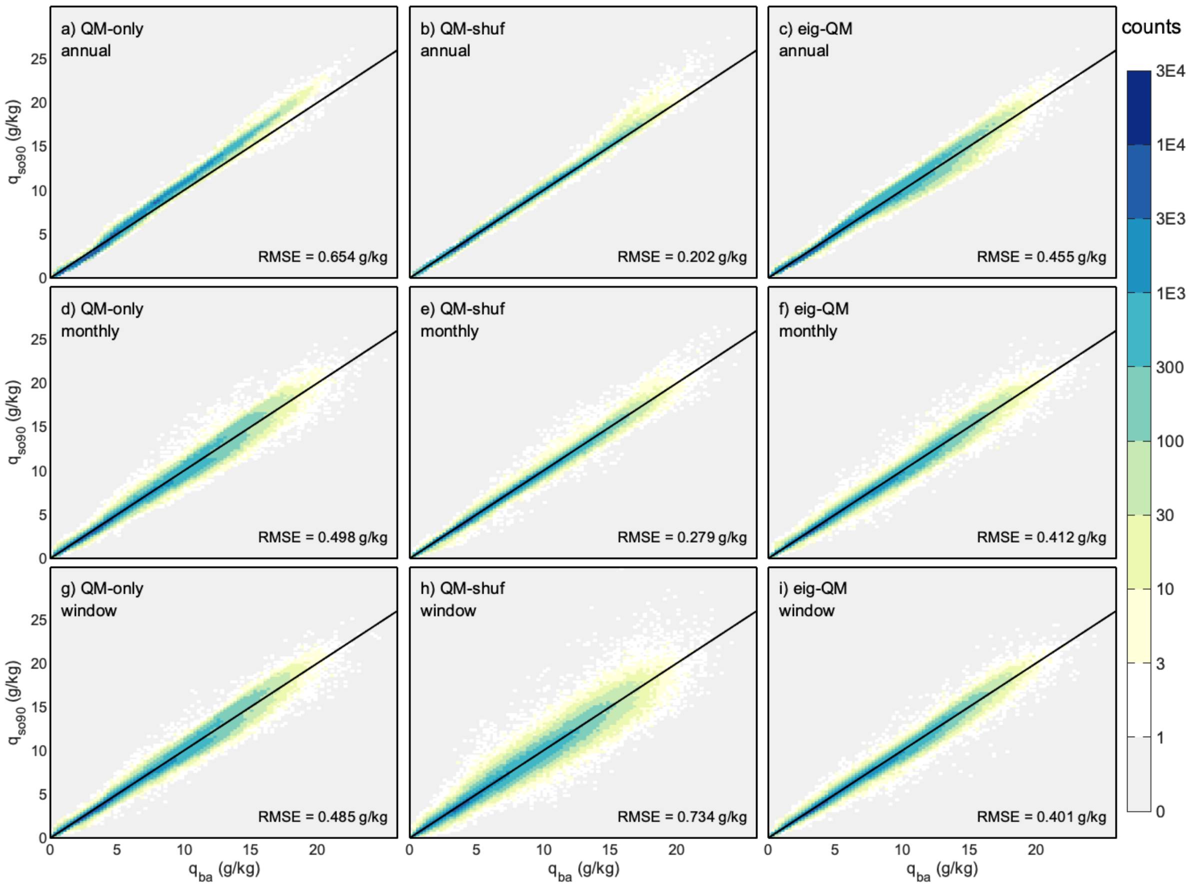


Figure 4: Two-dimensional counts for $q_{ba}$ and $q_{so90}$, for one study site (Montreal) and for 9 of the 18 alternative adjustment techniques (TP option is activated). Counts include the ten simulations over the full application period (1981-2100), for a total of 438,000 time steps. Bin size is 0.25 g/kg x 0.25 g/kg. Black lines indicate the 1:1 ratio. On each panel, the root-mean-square error (RMSE) between $q_{ba}$ and $q_{so90}$ is provided as a numerical indication of physical inconsistency (departure from the 1:1 ratio).

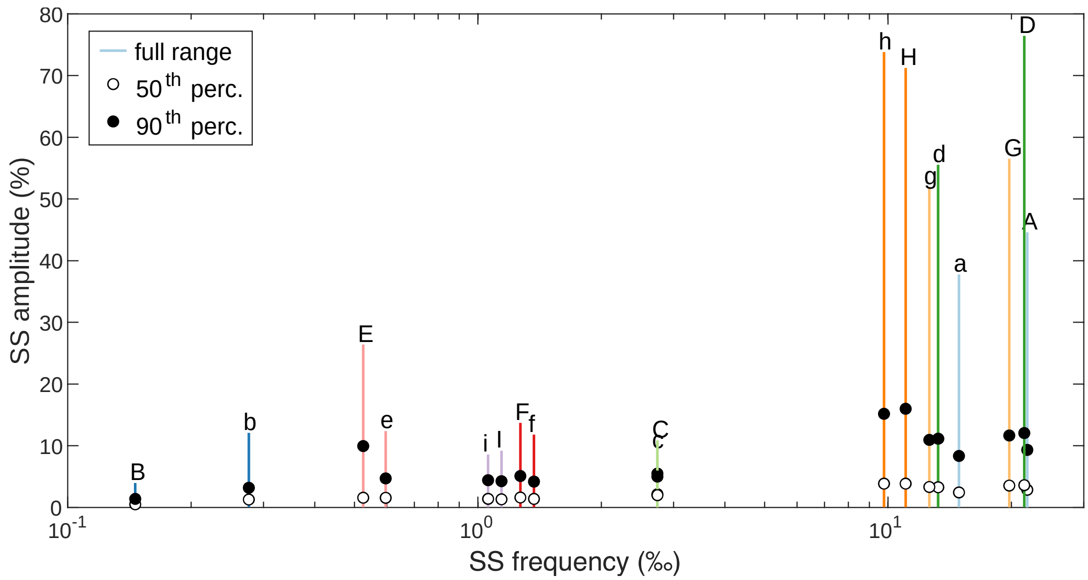


Figure 5: Frequency (per mil) and amplitude (%) of supersaturation (SS) occurrences in $RH_{so90}$, for one study site (Miami) and for each of the 18 bias adjustment techniques. Each distribution is built from the SS cases among 438,000 considered time steps (10 simulations over the application period 1981-2100), with the solid line positioned at the SS frequency (*x* axis) and extending over the full range of obtained SS amplitudes (along the *y* axis), and the empty (or filled) circle representing the $50^{th}$ (or $90^{th}$) percentile. Lowercase (or uppercase) letters are used to represent the deactivated (or activated) TP option, and the matching regarding the dimensionality and grouping options is the following: a/A for QM-only and annual; b/B for QM-shuf and annual; c/C for eig-QM and annual; d/D for QM-only and monthly; e/E for QM-shuf and monthly; f/F for eig-QM and monthly; g/G for QM-only and window; h/H for QM-shuf and window; i/I for eig-QM and monthly.

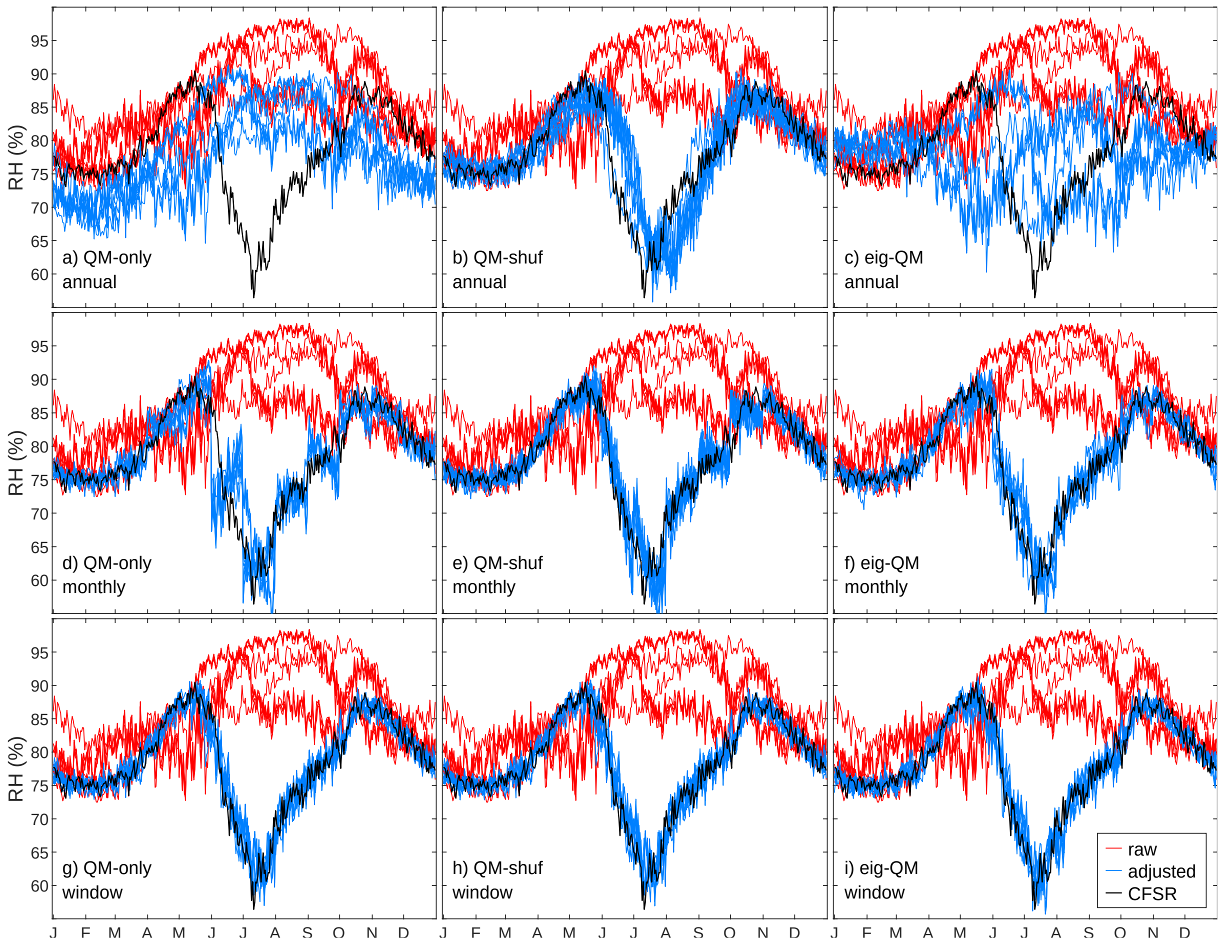


Figure 6: RH average annual cycle over the calibration period (1981-2010), for one study site (Iqaluit) and for 9 of the 18 alternative adjustment techniques (TP option is activated). The black line (corresponding to the reference product CFSR) and the red lines (each corresponding to one of the 10 raw simulations) are the same for all panels. Each blue line is the adjusted version of a raw simulation. Tick marks of the *x* axis indicate the first day of each month.

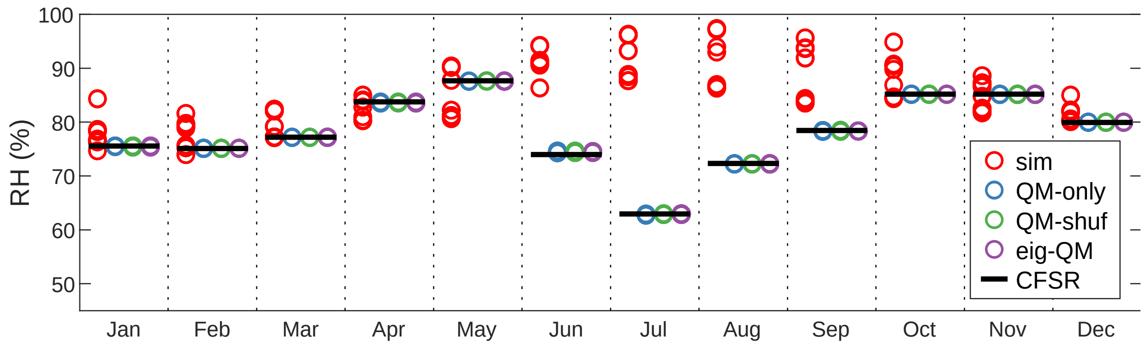


Figure 7: RH monthly average over the calibration period (1981-2010), for one study site (Iqaluit), for raw simulations (red), adjustment with QM-only (blue), adjustment with QM-shuf (green) and adjustment with eig-QM (purple). Each circle indicates one of the 10 (raw or adjusted) simulations (with superimposition in adjustment cases). Monthly grouping and TP options are activated. Black lines represent RH monthly averages for the reference product CFSR.

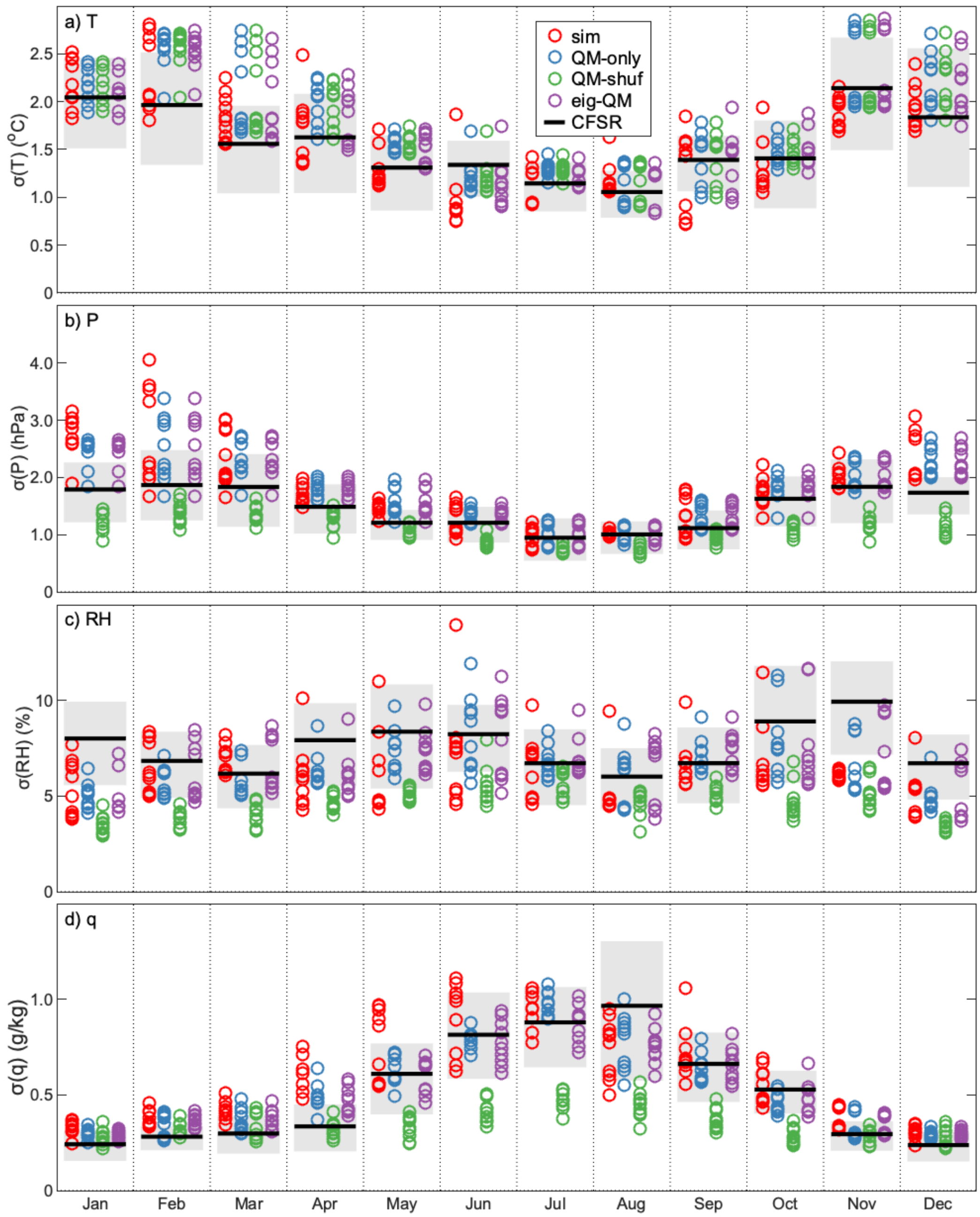


Figure 8: Standard deviation (σ) of monthly averages over the calibration period (1981-2010), for one study site (Denver), for variables: a) *T*; b) *P*; c) RH; and d) *q*. Each circle indicates one of the 10 (raw or adjusted) simulations, with same color code as in Figure 7. Window grouping and TP options are activated. Black lines represent CFSR σ values, and grey boxes delimit the 1$^{st}$ and 99$^{th}$ percentiles from 10,000 bootstrapping re-samplings of the 30 CFSR monthly averages.

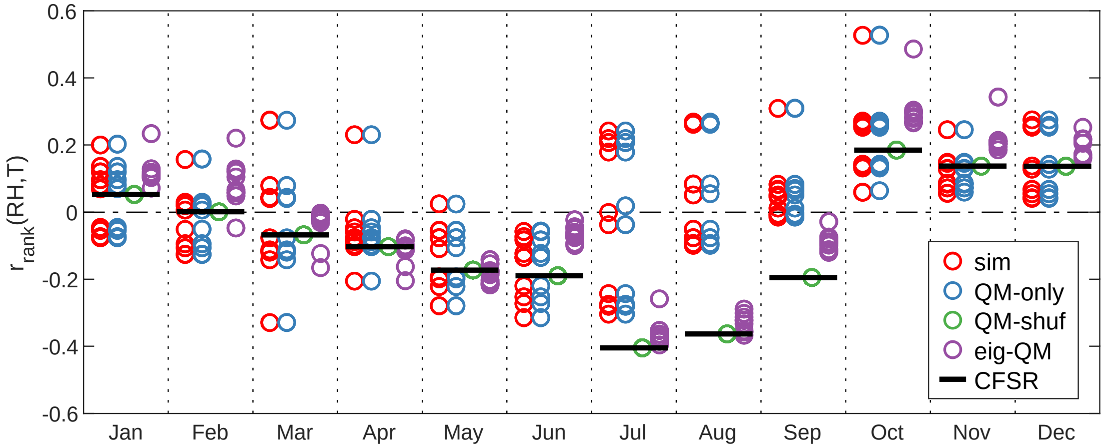


Figure 9: Spearman's (rank) correlation coefficient ($r_{rank}$) between RH and $T$, for all days in each month-of-the-year over the calibration period (1981-2010), for one study site (Mexico City). Each circle indicates one of the 10 (raw or adjusted) simulations, with same color code as in Figure 7. Window grouping is activated and TP is deactivated. Black lines represent CFSR $r_{rank}$ values.

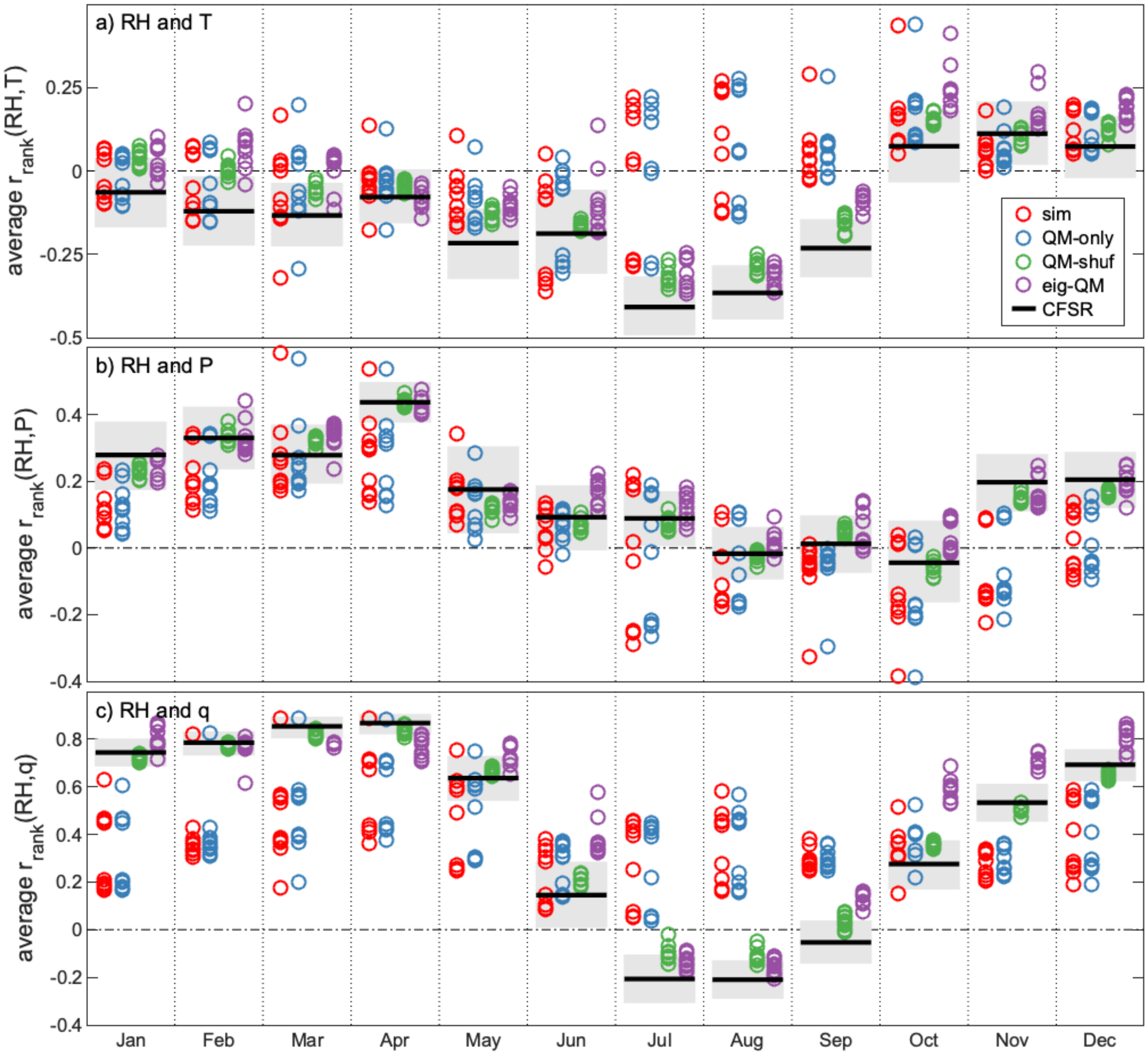


Figure 10: Average of the 30 intra-month $r_{rank}$ values over the calibration period (1981-2010), for one study site (Mexico City), for pairs of variables: a) RH and $T$; b) RH and $P$; and c) RH and $q$. Each circle indicates one of the 10 (raw or adjusted) simulations, with same color code as in Figure 7. Window grouping and TP options are activated. Black lines represent CFSR average intra-month $r_{rank}$ values, and grey boxes delimit the 1st and 99th percentiles from 10,000 bootstrapping re-samplings of the 30 CFSR intra-month $r_{rank}$ values.

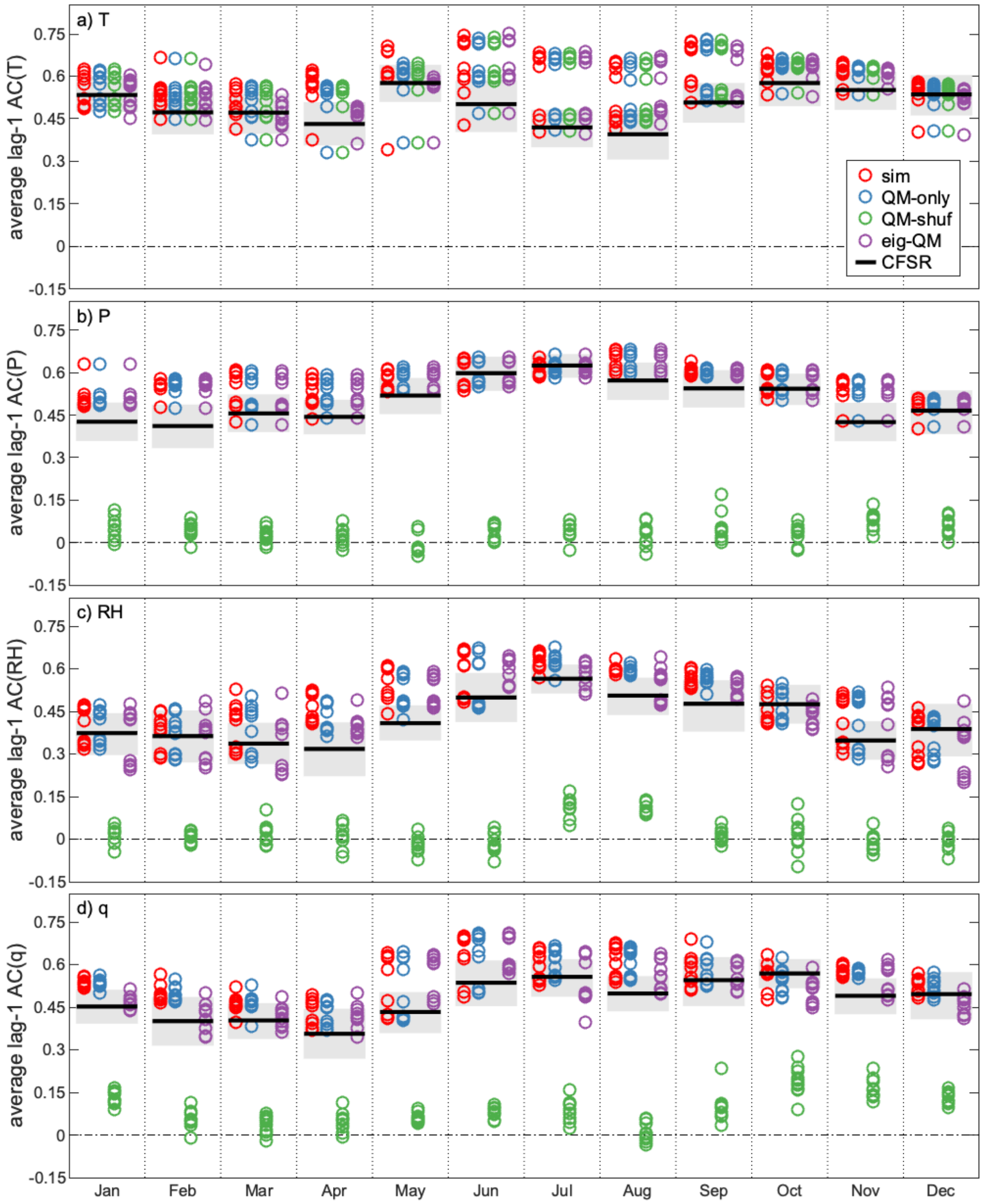


Figure 11: Average of the 30 intra-month lag-1 auto-correlation (AC) values over the calibration period (1981-2010), for one study site (El Paso), for: a) *T*; b) *P*; c) RH; and d) *q*. Each circle indicates one of the 10 (raw or adjusted) simulations, with same color code as in Figure 7. Window grouping and TP options are activated. Black lines represent CFSR average intra-month lag-1 AC values, and grey boxes delimit the 1st and 99th percentiles from 10,000 bootstrapping re-samplings of the 30 CFSR intra-month lag-1 AC values.

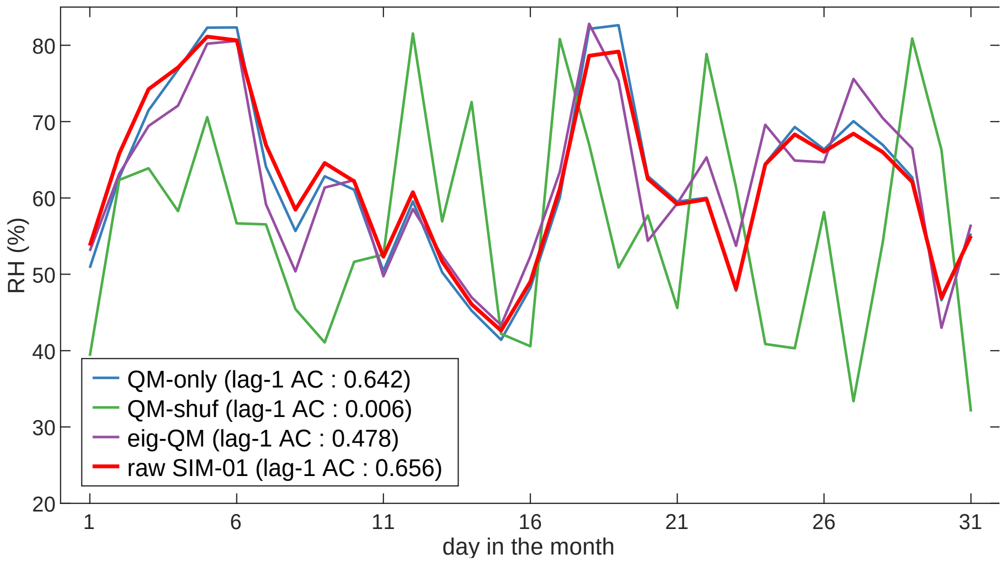


Figure 12: RH time series (at 12 UTC each day) for August 1981 at one site (El Paso), for raw SIM-01 and after different adjustments (window grouping and TP options activated in each case).

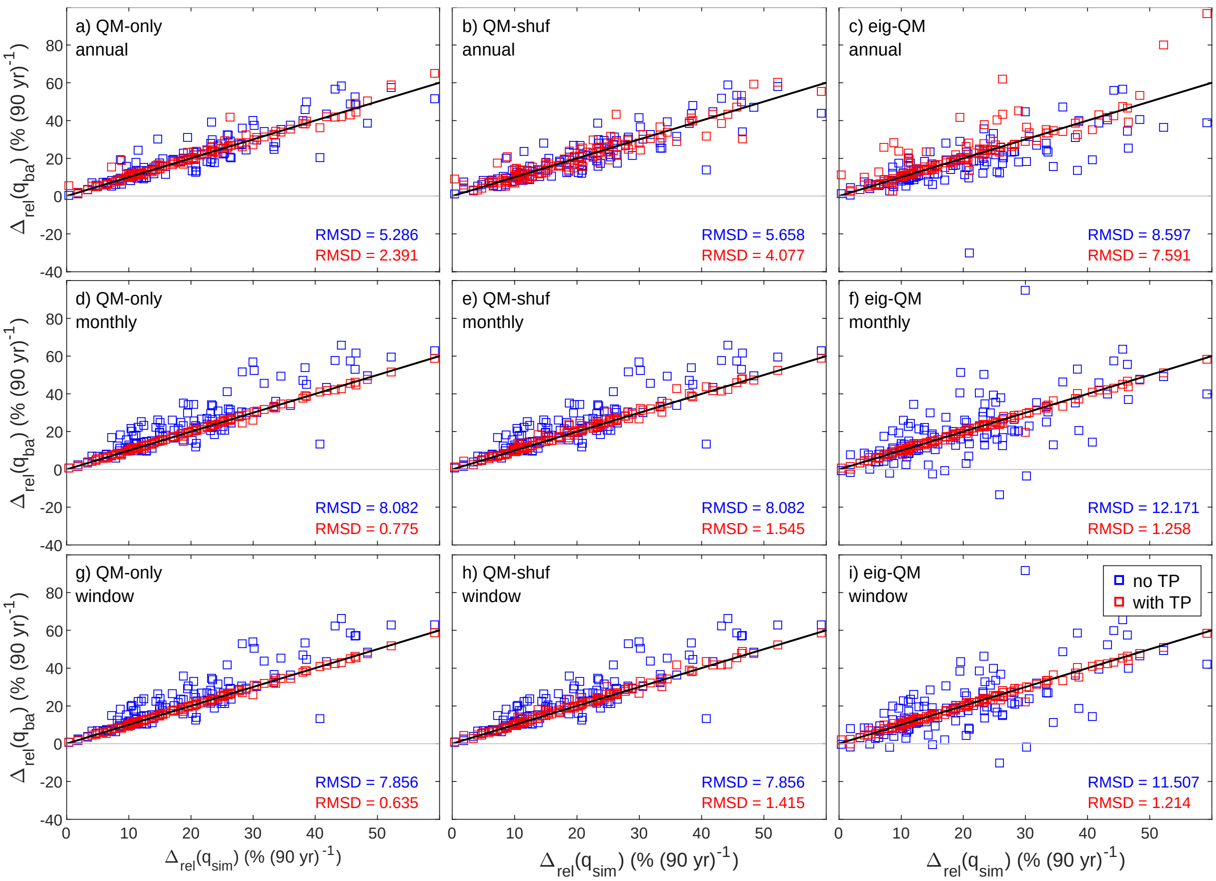


Figure 13: Relative long-term changes for September average specific humidity after adjustment, $\Delta_{rel}(q_{ba})$, in function of corresponding simulated changes, $\Delta_{rel}(q_{sim})$. Each panel contains 120 red symbols for adjustment with activated TP, and 120 blue symbols for adjustment without this procedure (12 sites x 10 simulations). Relative changes follow the general form [$\Delta_{rel}(q) \equiv 100(q(2071\text{-}2100) - q(1981\text{-}2010)) / q(1981\text{-}2010)$], in units of [% (90 yr)$^{-1}$]. Black lines indicate the 1:1 proportion, and printed root-mean-square differences (RMSD) are calculated over pairs of corresponding $\Delta_{rel}(q_{ba})$ and $\Delta_{rel}(q_{sim})$ values.

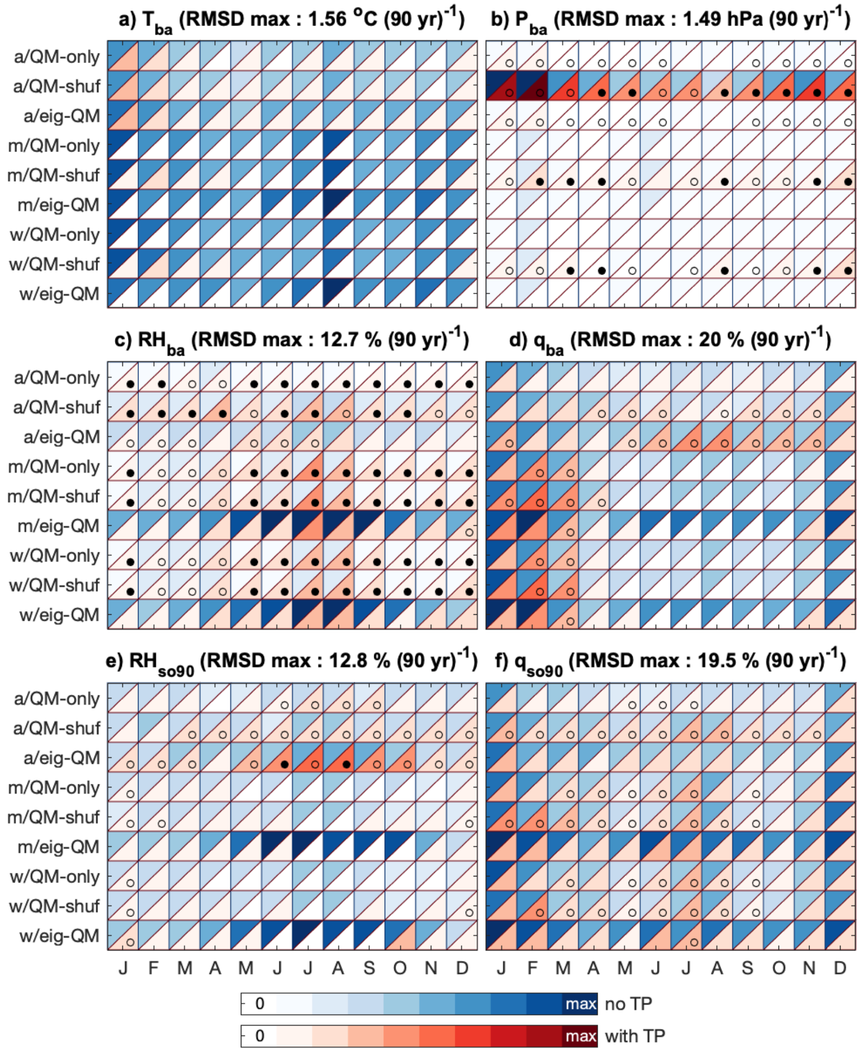


Figure 14: Root-mean-square differences (RMSD) over 120 pairs of corresponding bias-adjusted and raw simulated 1981-2010-to-2071-2100 change ($\Delta$ or $\Delta_{rel}$) values (12 sites x 10 simulations), for variables a) $T_{ba}$; b) $P_{ba}$; c) $RH_{ba}$; d) $q_{ba}$; e) $RH_{so90}$; and f) $q_{so90}$; and for all months (panel columns) and techniques (panel rows). Blue-shade upper-left (or red-shade lower-right) triangles correspond to technique without (or with) the trend preservation (TP) procedure. Labels ‘a’, ‘m’ and ‘w’ refer to annual, monthly and window grouping options, respectively. For each panel, RMSD values are presented as the fraction (white for 0 to 0.1, darker shade for 0.9 to 1) of the maximum of the 240 involved values. An empty (or filled) black dot indicates the associated with-TP RMSD value is larger than half its corresponding no-TP value (or larger than the corresponding no-TP value).

**END**